Received: 23 August 2020 | Revised: 5 July 2021 | Accepted: 16 July 2021 | Published on: 6 August 2021

DOI: 10.1002/joc.7304

RESEARCH ARTICLE

International Journal of Climatology RMetS

On the relationship between ENSO diversity and the ENSO atmospheric teleconnection to high-latitudes

Daria Gushchina[1,2] | **Maria Kolennikova**[1] | **Boris Dewitte**[3,4,5,6] | **Sang-Wook Yeh**[7]

[1]Faculty of Geography, Moscow State University (MSU), Moscow, Russia

[2]Russian State Hydrometeorological University (RSHU), St. Petersburg, Russia

[3]Centro de Estudios Avanzado en Zonas Áridas (CEAZA), La Serena, Chile

[4]Departamento de Biología, Facultad de Ciencias del Mar, Universidad Católica del Norte, Coquimbo, Chile

[5]Millennium Nucleus for Ecology and Sustainable Management of Oceanic Islands (ESMOI), Coquimbo, Chile

[6]CECI, Université de Toulouse, CERFACS/CNRS, Toulouse, France

[7]Marine Sciences and Convergent Technology, Hanyang University (ERICA), Ansan, South Korea

Correspondence
Daria Gushchina, Faculty of Geography, Moscow State University, Leninskie gory, 1, Moscow 119991, Russia.
Email: dasha155@mail.ru

Funding information
ANID (Concurso de Fortalecimiento al Desarrollo Científico de Centros Regionales 2020-R20F0008-CEAZA and Grant 1190276); Korean Meteorological Administration Research and Development Program, Grant/Award Number: KMI2020-01213; Russian Science Foundation, Grant/Award Number: 19-17-00198; ANR, Grant/Award Number: ANR-18-CE01-0012

Abstract

The El Niño-Southern Oscillation (ENSO) has experienced changes in its properties since the 1990s, particularly increased occurrence of Central Pacific El Niño events. These events have influenced atmospheric circulation in the mid to high-latitudes of both hemispheres through atmospheric teleconnection. Here it is shown that, in the Northern Hemisphere, the planetary circulation response to the Eastern Pacific (EP) event in boreal winter is associated with Rossby waves propagating poleward and is mostly confined to the Pacific region, while the Central Pacific (CP) event induces a negative phase of Arctic Oscillation (AO)-like circulation pattern at planetary scale. In the Southern Hemisphere (SH), the difference between the circulation patterns associated with the two types of El Niño in austral summer is rather small and the response of the tropospheric circulation consists of an Antarctic Oscillation (AAO)-like negative phase pattern. In the SH, the circulation response to CP Niño lasts longer than that to EP Niño. In particular, during EP Niño the composite circulation anomalies reverse sign from austral summer to winter, which is not the case during CP event. This adds an interhemispheric asymmetry dimension to the ENSO atmospheric teleconnection in the high-latitudes in relation to ENSO diversity. These changes in the circulation are associated with surface air-temperature anomalies that have the potential to exacerbate observed long-term trends. A subgroup of CMIP5 models that realistically simulate both ENSO nonlinearity (diversity) and the AO and AAO-like patterns are analysed, showing that in the warmer climate, the circulation response in the high-latitudes to both types of events is amplified in both hemispheres.

KEYWORDS

atmosphere circulation, ENSO, temperature anomalies, tropics-mid latitude teleconnection

1 | INTRODUCTION

Weather and climate variability in extra-tropical regions are influenced by tropical forcing. The main mode of tropical variability at the interannual timescale is the El Niño-Southern Oscillation (ENSO). Ocean warming associated with El Niño results in the release of large amounts of heat and moisture into the tropical free atmosphere that are then transferred to the mid-to-high latitudes via atmospheric teleconnections.

Theoretical and observational studies point to two main mechanisms for ENSO teleconnection in the

mid-to-high latitudes: a wave-train mechanism and an eddy-jet stream mechanism 2017. The former is an atmospheric response to steady thermal forcing near the equator in the form of Rossby wave trains emanating poleward from the tropics and arching eastwards (e.g., Hoskins and Karoly, 1981; Horel and Wallace, 1981; Trenberth *et al*., 1998). The eddy-jet stream mechanism reflects the changes in the strengths and locations of subtropical and polar jet streams resulting from ENSO impacts (Seager *et al*., 2003; L'Heureux and Thompson, 2006; Lu *et al*., 2008).

The Rossby wave train induced by abnormal heating in the tropical Pacific results in the dominant teleconnection pattern in the Northern Hemisphere (NH) known as the Pacific-North American Pattern (PNA). It manifests in quasi-stationary high and low pressure anomaly patterns, that is, strengthened Hawaii and Canadian highs, Aleutian low and Mexican depression (Leathers *et al*., 1991). The PNA is more pronounced in boreal winter when the tropical central/eastern Pacific (EP) heating associated with El Niño reaches its maximum and when westerly jet stream is shifted southward. In boreal summer the westerly jet stream weakens and shifts northward that reduce the forcing from equatorial heating, but the heating associated to the summer Asian monsoon can trigger the upper-level Asia–North America teleconnection pattern (Zhu and Li, 2016, 2018). Another NH teleconnection pattern is the North Pacific Oscillation (NPO), which has been related to Central Pacific El Niño (Di Lorenzo *et al*., 2010; Stuecker, 2018). The opposite anomalies of sea surface temperature (SST) in the eastern and central equatorial Pacific (cooling) may also generate the long barotropic Rossby wave, that force the large-scale pressure anomalies in the mid-latitude troposphere (Zhu *et al*., 2020). ENSO is not the unique source of Rossby wave train emanating from the tropics to the mid-to-high latitudes. For instance, Yan *et al*. (2021) show that wildfire aerosols emitted over tropical Africa can yield comparable wave train.

Both observational and model studies show evidence of the relationship between ENSO and main climate variability modes of NH extratropical circulation, that is, Arctic Oscillation (AO) and the North-Atlantic Oscillation (NAO). The energy from the tropics to the extratropical North Atlantic was shown to be transported through the tropical Atlantic SST (Rajagopalan *et al*., 1998; Robertson *et al*., 2000; Saravanan and Chang, 2000; Jia *et al*., 2009). However, the relationship between ENSO and AO is still debated. It is supposed that the strong ENSO/AO relationships are associated with the weak circumpolar vortex when the AO phases change with rather clear periodicity. The strong circumpolar vortex is mostly associated with the positive phase of AO and the linear relation between AO and ENSO are not present (Kryjov and Park, 2007). The latter agrees with the modelling study of Zhu and Wang (2016) showing that the correlation is low when AO and ENSO related signals are confined to high and low latitudes, respectively.

Several studies also examined the circulation response to ENSO in the Southern Hemisphere (SH; Rayner *et al*., 2003; Carvalho *et al*., 2005; L'Heureux and Thompson, 2006; Ciasto and Thompson, 2008; Pohl *et al*., 2010; Brands, 2017). ENSO accounts for ~25% of the Antarctic Oscillation (AAO) variability in austral summer during the peak of El Niño, and less during austral winter (L'Heureux and Thompson, 2006; Fogt and Bromwich, 2006). The positive (negative) ENSO phase is associated with the negative (positive) phase of AAO (van Loon and Madden, 1981; Karoly, 1989). However, the seasonality and impacts depend on the origin of the tropical Rossby wave train (Ding *et al*., 2012, 2016; Li *et al*., 2015).

While NH and SH teleconnections have been widely documented, the interhemispheric variability in ENSO response has been less studied. Carvalho *et al*. (2005) highlighted that, compared to the NH, the tropospheric response to the tropical forcing in the extra-tropics of the SH is characterized by deep and zonally symmetric or annular structures that represent exchanges of mass between the mid- and high-latitudes. While L'Heureux and Thompson (2006) evidence the interhemispheric asymmetry of the ENSO teleconnection consisting of different seasonality and location of zonal circulation anomalies, Ayarzagüena *et al*. (2018) note the seasonal dependence of the ENSO response in the Atlantic region where the interhemispheric symmetry is characteristic of early boreal winter and obvious asymmetry observed in the late winter.

The studies mentioned above provided a theoretical and observational framework for interpreting the ENSO-associated atmospheric teleconnection to the mid-to-high latitudes. However, they do not consider that large inter-event variability exists in terms of the ENSO teleconnection pattern (Zheleznova and Gushchina, 2015, Zheleznova and Gushchina, 2016; Yeh *et al*., 2018; Taschetto *et al*., 2020), even during extreme El Niño events (Dewitte and Takahashi, 2019). The details of the seasonal evolution of El Niño and where SST anomalies develop along the equator are fundamental for inferring atmospheric pathways and impacts (Frauen *et al*., 2014; Sanabria *et al*., 2018; Sulca *et al*., 2017; Cai *et al*., 2020).

This aspect of ENSO has been referred to in recent literature as ENSO diversity (Capotondi *et al*., 2015). Two main types of El Niño events are part of this ENSO diversity: the Central Pacific (CP) and the EP El Niño (Ashok *et al*., 2007; Kao and Yu, 2009; Kug *et al*., 2009). ENSO diversity can be also viewed in terms of the intensity of

the events (i.e., moderate vs. extreme/strong) with 'strong' El Niño events being the EP type (e.g., 1982/83, 1997/98), whereas CP El Niños are 'moderate' events (Takahashi and Dewitte, 2016). However, because during CP El Niño events the SST maximum is located near or within the warm pool where the well-developed deep convection takes place, the heat and moisture release to the atmosphere during a CP El Niño is such that the teleconnection pattern can be as marked as during strong EP El Niño events.

The difference of the atmospheric response to the two types of El Niño has been addressed in several studies. The pioneer study by Leathers *et al.* (1991) showed that the atmospheric response in the form of positive phase of PNA is the most prominent characteristic of EP El Niño events while El Niño events like the CP El Niño events were shown to be associated with the negative phase of North Atlantic Oscillation (NAO). The strong zonal subtropical jet tends to trap poleward propagating waves that then follow the subtropical waveguide (Ambrizzi and Hoskins, 1997; Branstator, 2002). During CP El Niño events, this subtropical bridge has been suggested to drive a zonally extended wave train from the Pacific to the Atlantic that is associated with a negative phase of the NAO (Graf and Zanchettin, 2012) and enhanced cyclogenesis in the Gulf Stream region (Schemm *et al.*, 2018). The related increased (Li and Lau, 2012) or more zonal (Drouard *et al.*, 2013) transient eddy propagation from the North Pacific to the North Atlantic has also been suggested to force a negative NAO phase (Jimenez-Esteve and Domeisen, 2018). The link between the western tropical Pacific forcing and the AO manifests in a positive anomaly of rainfall (Li *et al.*, 2006) and enhanced outgoing longwave radiation (OLR) (Zhou and Miller, 2005) associated with the low and high AO index, respectively.

In the SH, the response to the two types of El Niño exhibits a seasonal dependence: the EP El Niño favours the AAO-like negative phase circulation pattern in austral summer, while the CP El Niño promotes the negative phase of the AAO during the austral late autumn–winter (Lim *et al.*, 2013). The mechanisms of these teleconnection patterns are also distinct. In particular, the subtropical westerlies shift poleward during CP El Niño events, opposite to those during EP El Niño events, so that the westerly anomalies on the poleward flank of the subtropical jet act as a secondary source of baroclinic eddies in addition to the higher-latitude westerlies.

As a result, a source of the variability in the ENSO teleconnection arises from the modulation of ENSO itself manifested as the low-frequency change in the occurrence of CP and EP El Niño events observed over the last five decades (Lee and McPhaden, 2010; Takahashi *et al.*, 2011). In particular, the ENSO teleconnection has been shown to have changed since the 1990s when CP El Niño events became more frequent (Yeh *et al.*, 2018). Since the current generation of coupled models have some difficulties in simulating both ENSO diversity and mean state changes, and because the ENSO teleconnection is by essence non-linear (Frauen *et al.*, 2014), there is still a low confidence in projected changes in the ENSO teleconnection in a warmer climate (Yeh *et al.*, 2018; Taschetto *et al.*, 2020). Still, the models that tend to realistically simulate ENSO diversity project a significant increase in variance of EP El Niño events (Cai *et al.*, 2018; Carréric *et al.*, 2020) and, amongst these models, there is also a consensus on the pattern of the mean SST change (i.e., reduction of the zonal SST gradient across the equatorial Pacific caused by greater SST increase in the east than in the central and west Pacific) (Karamperidou *et al.*, 2017). Therefore the extent to which the models participating in the Coupled Model Intercomparison Project (CMIP) can provide material for better understanding the evolution of the ENSO teleconnection patterns in warmer climates still need to be evaluated. In particular, since the high-latitude systems are experiencing the largest warming trend on the planet (Larsen *et al.*, 2014), it is important to better understand how tropical interannual variability could exacerbate or mitigate those through the ENSO teleconnection (Grassi *et al.*, 2005).

Here we investigated the response of planetary scale atmosphere circulation to ENSO forcing in both hemispheres over the period 1950–2017 while taking into account the changes in ENSO properties over the last six decades. We also address the climate change issue based on a selection of 'realistic' CMIP5 climate models.

The article is organized as follows: first, the data and the methods are presented (Section 2). The Section 3 describes the response of planetary scale circulation to ENSO in the Northern and Southern Hemispheres based on the Reanalysis data, while the possible changes of the ENSO teleconnection in future climate are discussed in Section 4. Section 5 is a discussion followed by concluding remarks.

2 | DATA AND METHODS

2.1 | Data

The monthly geopotential at 1,000, 700 and 500 hPa (H1000, H700 and H500) and near surface air temperature were obtained from the NCEP/NCAR reanalysis (Kalnay *et al.*, 1996) for the period from 1950–2017. The Hadley Centre Global Sea Ice and Sea Surface Temperature (HadISST) archive was used to derive monthly SST

anomalies (Rayner *et al.*, 2003). As El Niño peaks during the boreal winter when the Artic Oscillation also has maximum amplitude, the data for December, January and February were examined for the NH. AAO has maximum amplitude in austral winter, therefore the teleconnection during June, July and August were analysed as well in the SH. The anomalies were calculated by removing seasonal cycles averaged over 1950–2017. All data were detrended before applying the lag-regression analysis.

To evaluate the dependence of the results on the data sets, the ERA-Interim reanalysis was also used (Dee *et al.*, 2011). It was shown (Figure S1) that the results obtained from NCEP/NCAR and ERA-Interim reanalyses are comparable for the overlapping period (1979–2015). The remainder of the article focuses on results derived from the NCEP/NCAR Reanalysis.

2.2 | Methods

The two ENSO indices introduced by Takahashi *et al.* (2011) were used. They account for the variability associated with the EP El Niño and the CP El Niño events (here after E and C indices) and are defined based on the first two EOF modes of SST data over the tropical Pacific (11°S–11°N; 120°E–80°W). They consist of the linear combination (through rotation) of the principal components of the first two EOFs—PC1 and PC2. Whereas the E index accounts for the extreme El Niño events that are of the EP type, the C index captures the variability associated with the CP El Niño and La Niña events. These indices are independent by construction (i.e., their correlation is zero) and can be conveniently used for regression analysis. To determine the spatial pattern of SST anomalies associated with each index, the bilinear regression of SST anomalies over the tropical Pacific (20°S–20°N; 120°E–80°W) onto E (E-pattern) and C (C-pattern) indices was used.

For composite analysis, the CP and EP years were selected using the method proposed by Yeh *et al.* (2009). If the Niño3 index (SST anomaly [SSTA] averaged over Niño3 region [5°S–5°N; 150°–90°W]) is greater than 0.5°C and the Niño4 index [SSTA averaged in Niño4 region (5°S–5°N, 160°E–150°W)] for three consecutive months or more from October to March, then the EP El Niño is occurring. If the Niño4 index is greater than the Niño3 index and 0.5°C, then the CP El Niño is identified. Over 1950–2017, this leads identification of five CP events (1968–1969, 1990–1991, 1994–1995, 2004–2005, 2009–2010) and 7 EP events (1965–1966, 1972–1973, 1976–1977, 1982–1983, 1991–1992, 1997–1998, 2015–2016).

The AO was defined as the first EOF mode of the monthly 1,000 (500) hPa geopotential height anomalies poleward of 20°N (Thompson and Wallace, 1998). The AAO was defined as the first EOF mode of the monthly 700 (500) hPa geopotential height anomalies poleward of 20°S (http://www.bom.gov.au/climate/enso/history/ln-2010-12/SAM-what.shtm).

We analysed 17 climate models from the Coupled Model Intercomparison Project phase 5 (CMIP5) that exhibited skill in simulating realistic ENSO properties (Table 1). In particular, these models capture nonlinearity in ENSO properties that is a good metric of the ability of the models to realistically simulate the two types of El Niño events (Cai *et al.*, 2018). The data of two experiments were used: 'historical' and Representative Concentration Pathway (RCP) 8.5 Data from the 'historical' experiment covers the period from 1916 to 2005 and consists of simulations where the observed changes in air composition (including CO_2) was due to both anthropogenic and volcanic impacts, and the radiative forcing was associated with the release of short-lived natural and anthropogenic aerosols into the atmosphere. Land use and its impact on greenhouse gas emission were also considered (Taylor *et al.*, 2012). The RCP8.5 scenario corresponds to a high greenhouse gas emissions pathway. The greenhouse gas emissions and concentrations in this scenario considerably increase over time, leading to a radiative forcing of 8.5 $W \cdot m^{-2}$ at the end of the 21st century. It covers the period from 2006 to 2095.

To diagnose the changes in ENSO statistics in the future climate, we compare the E and C modes for the two periods: 1916–2005 from historical experiment and 2006–2095 from RCP8.5 experiment. The changes in statistics are reflected in both the pattern and the temporal evolution of the modes. To take into account the change of ENSO patterns between the present and future climate, the E and C indices of the RCP8.5 simulations were scaled by the projection of the associated spatial pattern on its counterpart of the historical run as in Carréric *et al.*, 2020.

3 | ATMOSPHERE CIRCULATION RESPONSE TO TWO TYPES OF EL NIÑO IN THE MODERN CLIMATE

3.1 | Northern hemisphere

To examine the circulation patterns associated with the two types of ENSO, the composites of geopotential anomalies at 1,000 hPa during EP and CP events and regression of H1000 against the E and C indices were plotted (Figure 1). First, we focused on the synchronic regression because the characteristic propagation time of the poleward wave that responds to El Nino lasts for only a couple of weeks (Thompson *et al.*, 2000; Kryjov and Gorelits,

TABLE 1 CMIP5 climate models used in the current investigations

No	Model	Country	Resolution
1	bbc-csm1-1-m	Beijing Climate Center, China Meteorological Administration, China	2.8125° × 2.7906°
2	CCSM4	National Center for Atmospheric Research, USA	1.25° × 0.9375°
3	CESM1-BGC	Community Earth System Model Contributors, USA	1.25° × 0.9375°
4	CESM1-CAM5	Community Earth System Model Contributors, USA	1.25° × 0.9375°
5	CMCC-CESM	Centro Euro-Mediterraneo per I Cambiamenti Climatici, Italy	3.75° × 3.75°
6	CMCC-CM	Centro Euro-Mediterraneo per I Cambiamenti Climatici, Italy	0.75° × 0.75°
7	CMCC-CMS	Centro Euro-Mediterraneo per I Cambiamenti Climatici, Italy	3.75° × 3.7111°
8	CNRM-CM5	Centre National de Recherches Météorologiques/Centre Européen de Recherche et Formation Avancée en Calcul Scientifique, France	1.40625° × 1.40625°
9	FIO-ESM	The First Institute of Oceanography, SOA, China	2.8125° × 2.8125°
10	FGOALS-s2	LASG, Institute of Atmospheric Physics, Chinese Academy of Sciences, China	2.8125° × 1.6590°
11	GFDL-CM3	NOAA Geophysical Fluid Dynamics Laboratory, USA	2.5° × 2.0°
12	GFDL-ESM2M	NOAA Geophysical Fluid Dynamics Laboratory, USA	2.5° × 2.0°
13	GISS-E2-H	NASA Goddard Institute for Space Studies, USA	2.5° × 2.0°
14	GISS-E2-R	NASA Goddard Institute for Space Studies, USA	2.5° × 2.0°
15	IPSL-CM5B-LR	Institute Pierre-Simon Laplace, France	3.75° × 1.875°
16	MIROC5	Atmosphere and Ocean Research Institute (The University of Tokyo), National Institute for Environmental Studies, and Japan Agency for Marine-Earth Science and Technology, Japan	1.40625° × 1.40625°
17	MRI-CGCM3	Meteorological Research Institute, Japan	1.125° × 1.125°

2015) while the resulting circulation anomaly persists over the whole winter and more. The composite circulation pattern of CP El Niño events is characterized by positive anomalies over the Arctic basin with two maxima located over the North Eurasia and North Atlantic/South Greenland. Low surface pressure was observed over the mid-latitudes with three maxima located in the extratropical Pacific and Atlantic and over the South-Eastern Asia (Figure 1a). The observed geopotential distribution is similar to the circulation pattern of a negative phase of the AO (Figure 1e) with the spatial correlation between them reaching .52. The difference in the atmospheric circulation between the CP El Niño associated pattern and the AO consists mostly of the larger extension of positive geopotential anomalies towards the mid-latitudes during the CP El Niño events compared to the maximum of AO pattern centred over the North Pole. Moreover, the main negative minimum in the CP El Niño composite is located over the Pacific and over the Atlantic in the AO pattern. The minimum is also shifted eastward to the North America coast during CP events as compared to AO. This difference is due to the fact that despite the atmospheric teleconnections being driven by the tropical convective forcing associated with CP El Niño, there exists some similarities in the spatial structure of AO which is an intrinsic atmosphere circulation in the mid-to-high latitudes.

The regression map of H1000 onto the C index showed a structure similar to the negative phase of AO (Figure 1c,e) with an even higher level of spatial correlation (.68). Notably, the CP El Niño composite was slightly different from the regression pattern because the regression analysis tends to emphasize the teleconnection pattern associated with the season when the C index peaks (i.e., December–January–February). On the composite map, the positive geopotential anomalies encompass the mid-latitudes with a maximum over Europe and the Atlantic (Figure 1a), while on the regression map, they are more confined to the polar and subpolar regions (Figure 1c). Despite these differences between the composite and regression analyses, the overall correspondence in the ENSO teleconnection patterns provides some confidence in the significance of the differences between circulation response to CP and EP El Niño events. Since the C index accounts for variability associated with both CP El Niño (positive values) and La Niña (negative values) events (Takahashi *et al.*, 2011), we also checked that the regression pattern associated with the positive C index is comparable to when negative values are not discriminated (not shown), which indicates that the AO-like

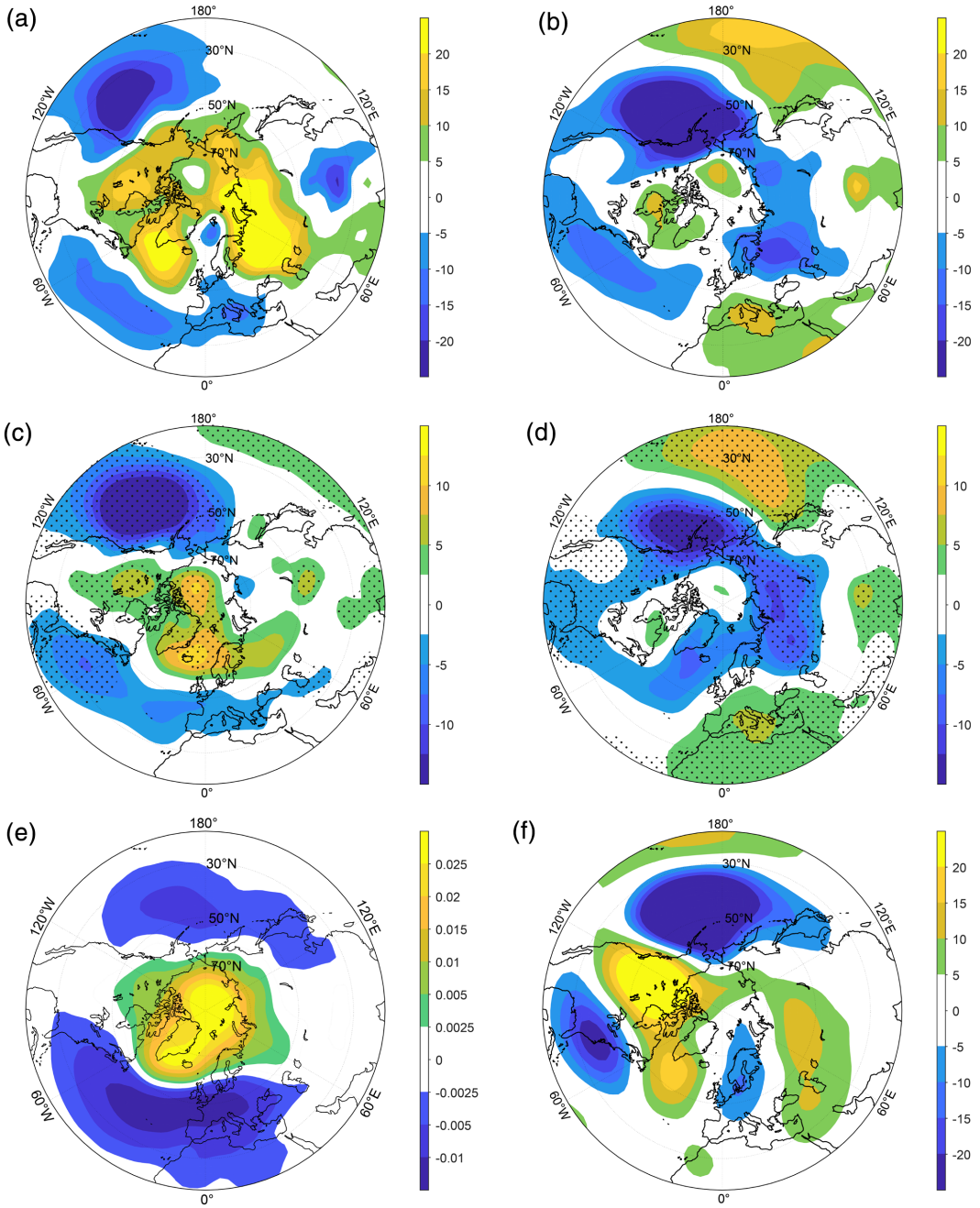

FIGURE 1 Composite maps of geopotential height anomalies at 1,000 hPa level in boreal winter for Central Pacific (a) and Eastern Pacific (b) El Niño events. Regression of geopotential height anomalies at 1,000 hPa level in boreal winter on C index (c) and E index (d). Dotted areas represent statistically significant values at a 90% confidence level. Negative phase of Arctic Oscillation at 1,000 hPa level (e). Positive phase of PNA (f). Contour interval is 5 hPa in panels (a,b,f), 2.5 hPa in panels (c,d) and 0.005 hPa in panel (e). The outermost latitude is 20°N [Colour figure can be viewed at wileyonlinelibrary.com]

response is characteristic of that of CP El Niño events (Figure 1c).

The EP composite and regression of H1000 onto the E-index (Figure 1b,d) exhibits a wave structure and is reminiscent of the PNA pattern (Figure 1f). In particular, the long Rossby wave propagating from the tropics manifests in an enhanced Hawaii high, Aleutian low, Canadian high and Mexican depression with maximum anomalies over the Pacific Ocean. This result agrees with previous studies showing that the abnormal heat release in the equatorial Pacific associated with El Niño induces the PNA-like wave response in the atmosphere of the NH (Trenberth *et al.*, 1998). Over Eurasia, the circulation response to

the EP El Niño manifests in low pressure anomalies centred over Siberia (Figure 1b,d).

As the Rossby waves have stronger amplitude in the middle and upper troposphere, the regression of geopotential at 500 hPa onto the El Niño indices was also analysed (Figure 2). The regression patterns at H500 are similar to those obtained for the low troposphere but with more pronounced annular (wave) structure for the CP (EP) events. During CP events, the mid-latitude low pressure belt is broken over middle Eurasia (Figure 2a), which is similarly observed in the AO pattern at the 500 hPa level (Figure 2b). The EP El Niño-associated circulation pattern represents the wave with zonal wavenumber 3 with maximums over North-East America, Central Europe and Far East and minimums located over the North Pacific, Atlantic and Ural region (Figure 2c).

Circulation anomalies, such as the AO, NAO, PNA and others, result in significant temperature anomalies around the world. The AO negative phase is associated with the weakening of westerlies and increased invasion of Arctic air into the mid-latitudes resulting in cold winters in Eurasia and North America (Thompson and Wallace, 1998). The positive PNA phase induces positive temperature anomalies over North-Western America and negative anomalies over Greenland and EP (Leathers *et al.*, 1991). To identify the temperature anomalies related to the circulation anomalies associated with the two types of El Niño, the regression of near surface temperature onto the E and C indices was calculated. CP events are associated with warmer conditions over the EP and western coasts of North America (Figure 3a), while colder conditions are observed over the central and North Eurasia, central and western Pacific and eastern coasts of North America. The maxima are centred over Alaska and Greenland and the minimum over the southeast USA, the Siberian Arctic, Kamchatka and the CP. These anomalies are strongly consistent with the temperature response associated with the negative phase of the AO. During EP events, the negative temperature anomalies are located over the Arctic and positive anomalies over the central part of Eurasia and North America. This pattern may result from enhanced mean western currents that advect warm air on the continents and isolate cold air in the Arctic region (Figure 3b). Notably, over a large part of the NH, the values of the regression coefficient of air temperature onto the C and E indices are generally opposite, except over the Pacific, Alaska and Eastern Siberia where the temperature response to both types of El Niño has the same sign (Figure 3).

Next, the 1- and 2-month lagged-regression between ENSO indices and geopotential during the months of December–March were analysed (Figure 4). Values for the lag were selected assuming that the circulation over the mid-to-high latitudes exhibits drastic change from winter to spring that could camouflage the remote signal. Note that the regression of January–February H1000 onto December–January El Niño indices does not significantly differ from simultaneous regression but significant differences emerge when the March circulation is regressed onto the winter indices (Figure 4d,h). In March, following CP events, the negative pressure anomalies are confined to the Polar region, while in the Pacific the Hawaii maximum is intensified. In contrast, in March following the EP El Niño peak, the subtropical Pacific maximum disappears and the main positive regression is located over Asia. Arguably these changes of atmosphere circulation lagged response are mostly due to the spring reorganization of the circumpolar vortex and associated changes of troposphere circulation in Polar region that

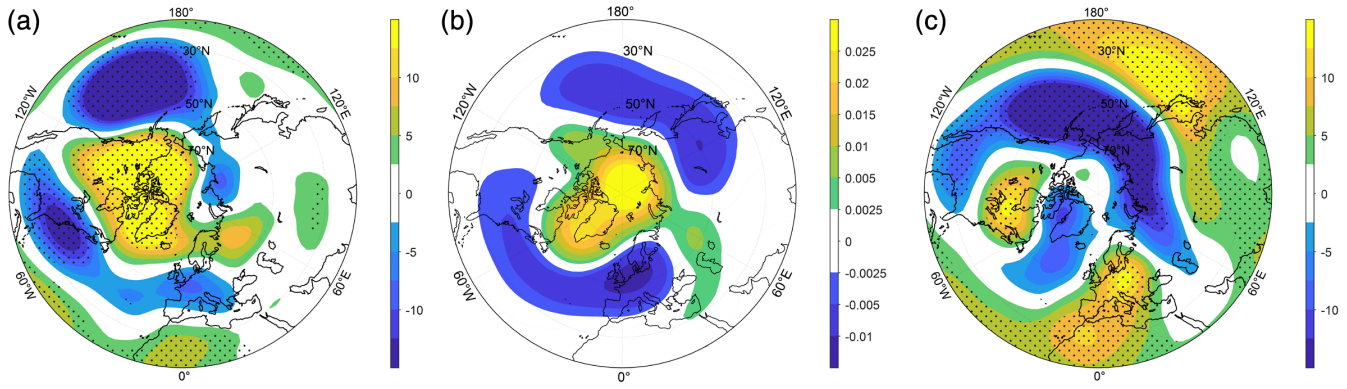

FIGURE 2 Regression of geopotential height anomalies at 500 hPa level in boreal winter on C index (a) and on E index (c). Dotted areas represent statistically significant values at a 90% confidence level. Negative phase of Arctic Oscillation at 500 hPa level (b). Contour interval is 2.5 hPa in panels (a,c) and 0.005 hPa in panel (b). The outermost latitude is 20°N [Colour figure can be viewed at wileyonlinelibrary.com]

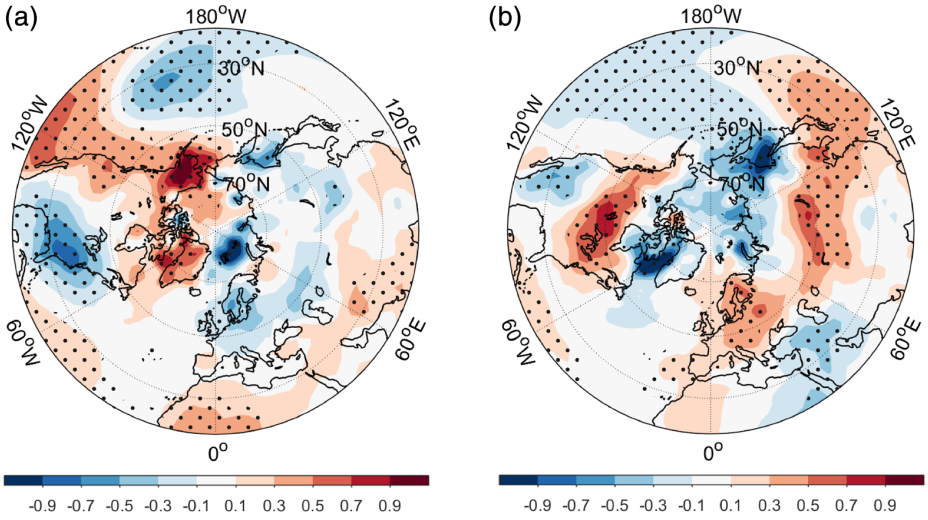

FIGURE 3 Regression of surface air temperature anomalies in boreal winter on C index (a) and E index (b). Dotted areas represent statistically significant values at the 90% confidence level. Contour interval is 0.2°C. The outermost latitude is 20°N [Colour figure can be viewed at wileyonlinelibrary.com]

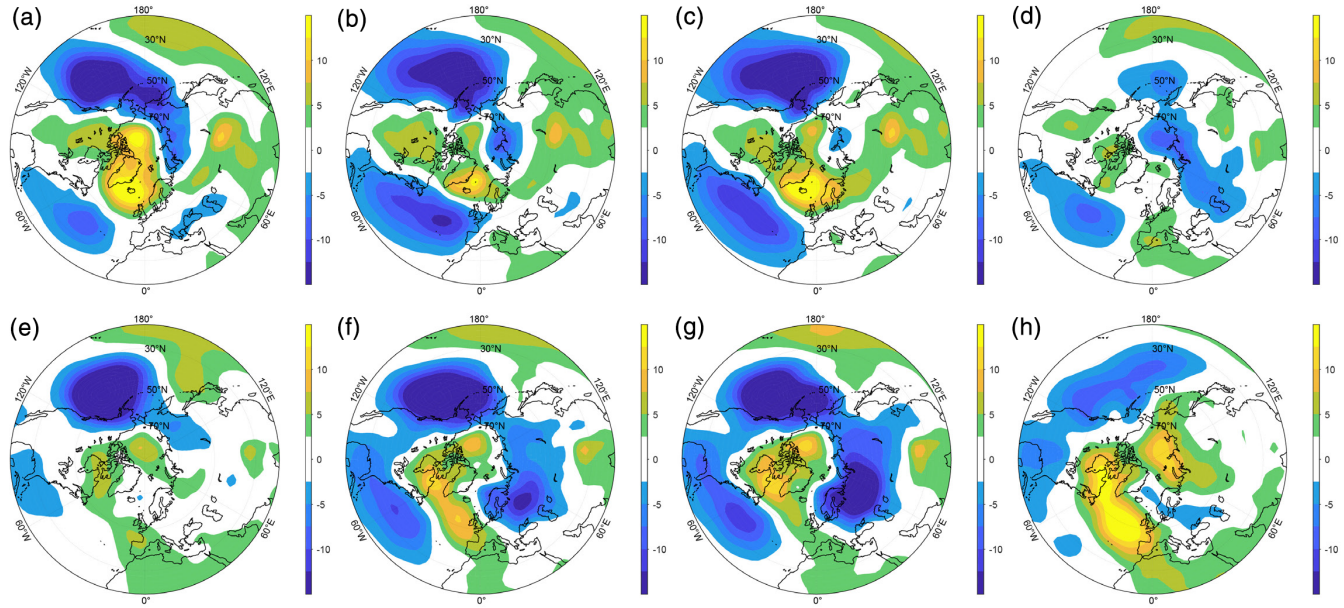

FIGURE 4 Lag regression of geopotential height anomalies at 1,000 hPa level on C index (a–d): (a) December–January, (b) December–February, (c) January–February, (d) January–March. The first month corresponds to the ENSO index and the second month to geopotential anomalies. The same is shown here but for regression on E index (e–h). Contour interval is 2.5 hPa. The outermost latitude is 20°N [Colour figure can be viewed at wileyonlinelibrary.com]

result in weaker sensitivity to the tropical forcing (Baldwin, 2019).

3.2 | Southern hemisphere

The SH response to the two types of El Niño was analysed based on composite and regression analysis similar to the NH analysis. The composites of geopotential at 700 hPa and AAO negative phase pattern are presented (Figure 5) along with the regression of H700 onto ENSO indices in austral summer and winter (Figure 6). The regression for H500 was also calculated but, due to its similarity with that of H700, it is not presented. For the NH, we focused on the analysis of the circulation response in boreal winter because El Niño usually peaks in November–January when the maximum of the AO occurs. However, for the SH, since El Niño usually starts to develop in austral winter when the AAO tends to be at its peak and El Niño peaks during austral summer when AAO amplitude is weaker, we carried out the analysis for both seasons (austral winter and summer). The simultaneous regressions for austral winter and austral summer, as well as the regression between December–January–

February (DJF) ENSO indices and geopotential in June–July–August (JJA), were calculated.

The composites presented in Figure 5 indicate that the circulation pattern in austral summer during the EP El Niño event resembles that of the negative phase of AAO (spatial correlation reaches .68; Figure 5b,f), consistent with previous studies (Seager *et al.*, 2003). The positive geopotential anomalies associated with the EP event are located over the Antarctica while the negative pressure anomalies are located in the mid-latitudes. The centre of maximum positive anomalies is shifted from the continent towards the Pacific by ~20° as compared to the AAO pattern. The CP El Niño composite notably differs from that of EP El Niño. In particular, the DJF composite displays positive anomalies in the subtropics and low pressure in the subpolar and polar regions

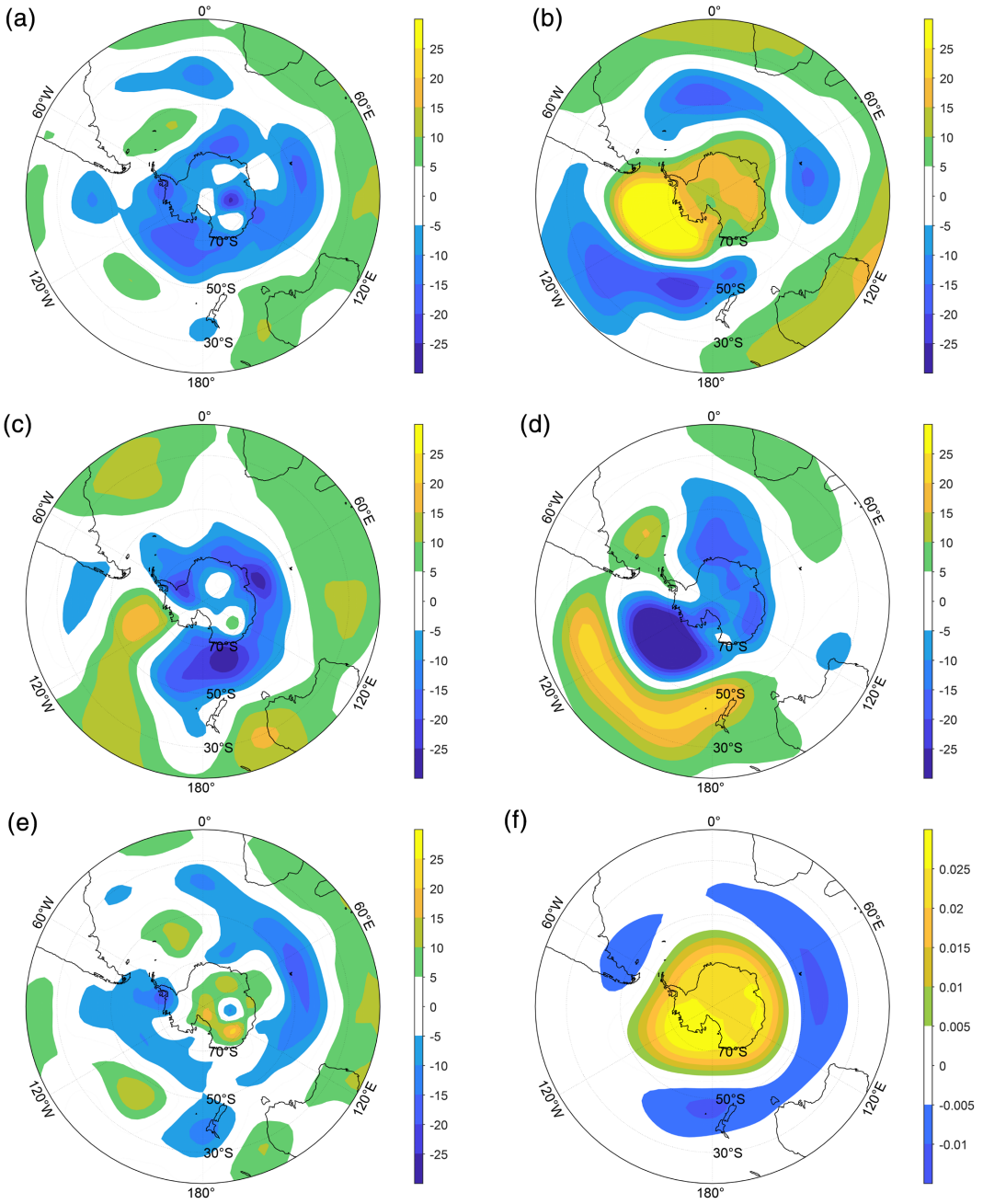

FIGURE 5 Composite maps of geopotential height anomalies at 700 hPa level in austral summer for Central Pacific (a) and Eastern Pacific (b) El Niño events. Composite maps of geopotential height anomalies at 700 hPa level in austral winter following Central Pacific (c) and Eastern Pacific (d) El Niño events. Composite map of geopotential height anomalies at 700 hPa level in austral summer for Central Pacific El Niño events except for El Niño 1994–1995 (e). Negative phase of Antarctic Oscillation at 700 hPa level (f). Contour interval is 5 hPa in panels (a–e) and 0.005 hPa in panel (f). The outermost latitude is 20°S [Colour figure can be viewed at wileyonlinelibrary.com]

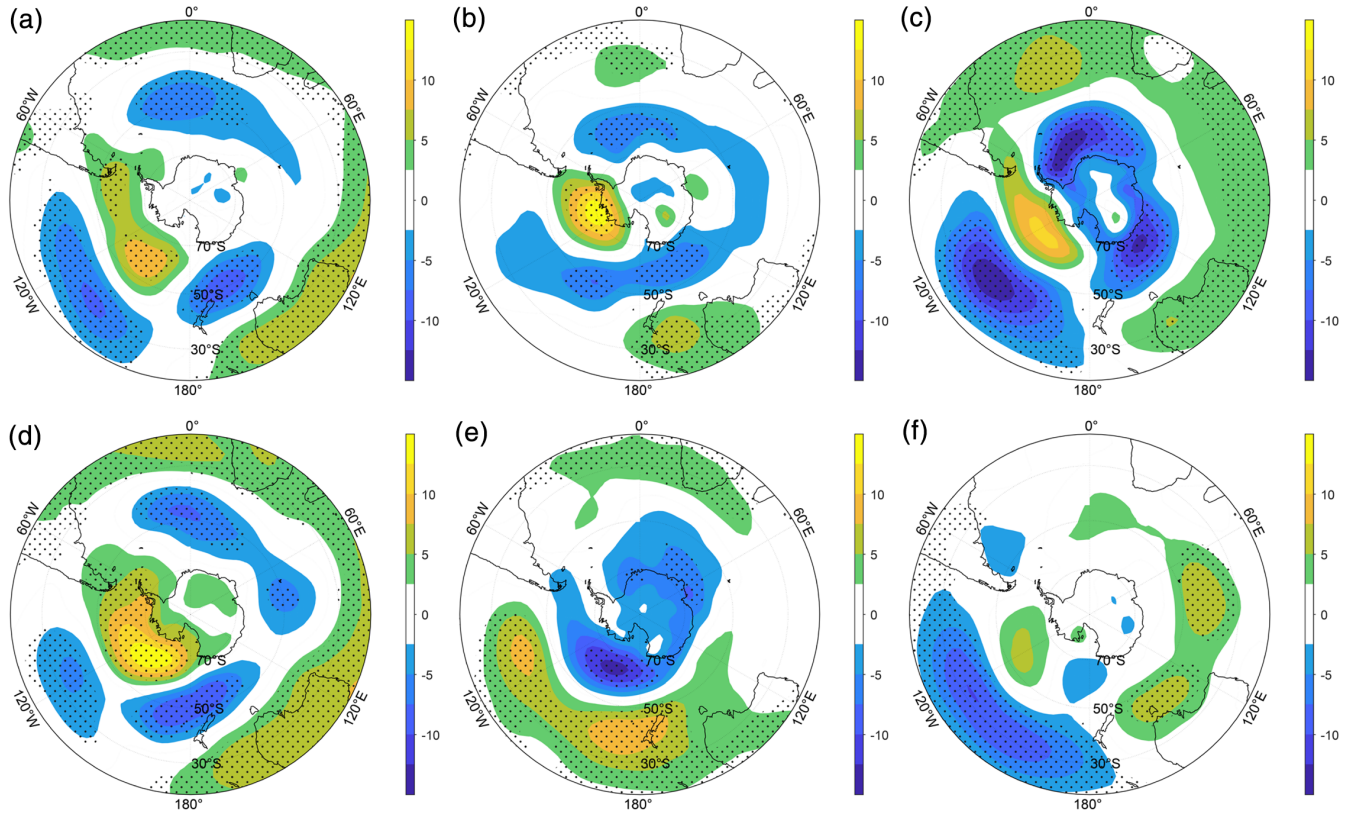

FIGURE 6 Regression of geopotential height anomalies at 700 hPa level on C index (a–c): (a) austral summer—austral summer, (b) austral summer—following austral winter, (c) austral winter—austral winter. The first season corresponds to the ENSO index and the second season to geopotential anomalies. The same is shown here but for regression on E index (d–f). Dotted areas represent statistically significant values at a 90% confidence level. Contour interval is 2.5 hPa. The outermost latitude is 20°S [Colour figure can be viewed at wileyonlinelibrary.com]

(Figure 5a), which is more similar to the positive AAO phase. However, inspection of individual El Niño events indicates that the inversed distribution of geopotential anomalies is mostly due to the 1994–1995 austral summer that was associated with dramatic negative anomaly located over Antarctica. When this El Niño event is excluded from the composite analysis, the composite map for CP El Niño is more like the negative AAO distribution (Figure 5e,f). These huge anomalies in H700 over Antarctica during the 1994–1995 austral summer could be associated with the nonlinear interaction between the forced response to ENSO and the internal unforced atmospheric variability of the Southern Annular Mode promoted by air-sea-ice interactions but it is beyond the scope of the present study to investigate this issue.

The simultaneous regression of H700 onto the E index in DJF is alike the composite and also displays a pattern similar to that of the negative AAO (spatial correlation of .44), although the maximum is not centred over the pole but is shifted towards 65°S (Figure 6d). During CP events, the location of positive regression coefficients is shifted even more equatorward over the Pacific as compared to during EP events, corresponding to a weakening of the subpolar depressions over the Pacific (Figure 6a).

Therefore, by comparing the SH and NH DJF circulation response, we may conclude that the difference between El Niño types is less pronounced in the SH with both types of events being associated with a prominent annular structure similar to that of the AAO. However, the symmetrical structure centred over the South Pole, which is a typical structure of the AAO, is not observed in both types of El Nino events and the maximum anomalies are shifted towards the Pacific Ocean.

The composite for austral winters following the EP El Niño peak is almost opposite to that of the summer (Figure 5b,d) and is similar to the positive phase of AAO with negative geopotential anomalies over the pole, indicating intensified circumpolar vortex and positive anomalies in the subtropics and the mid-latitudes. However, the AAO is characterized by an annular symmetrical structure while the ENSO-teleconnection pattern has marked longitudinal variability. The CP El Niño composite in austral winter is not the exact opposite to that in austral

summer but both differs significantly (Figure 5c,e). In JJA, the positive anomalies over the pole are weak and limited in space, the negative anomalies are shifted from the Southern Ocean toward Antarctica, and the strong positive anomaly appears over the Bellingshausen Sea. As a result, the austral winter CP composite is alike the positive phase of AAO.

The simultaneous regression of geopotential onto ENSO indices in JJA is similar to the regression in DJF for the CP event and differs significantly for EP events. In austral winters following a CP El Niño peak, positive regression coefficients of geopotential height at 700 hPa onto C index are located over subpolar and mid-latitudes over the Pacific and negative regression coefficients are observed between 70°S and 40°S over the Indian and Atlantic Oceans and to the north of 50°S over the Pacific Ocean (Figure 6c). This structure is comparable to that of the DJF regression map although the latter is characterized by values of regression coefficient almost half that of the JJA. This points to a stronger SH circulation response to ENSO observed in austral winter. The simultaneous regression patterns in JJA following EP events are similar to those of DJF over the Western Hemisphere and are opposite over the Eastern Hemisphere (Figure 6f) with positive (negative) anomalies dominating over the Southern Ocean in austral winter (summer).

Notably, the lagged response of the circulation to EP El Niño significantly differs from the instantaneous response that is not seen during CP events (Figure 6). The circulation anomalies associated with the CP El Niño are rather persistent; the regression patterns do not change when simultaneous winter or summer regression or lagged regression of the JJA geopotential onto the DJF C index is considered (Figure 6a–c). This is likely due to the longer persistence of SST anomalies during CP El Niño events compared to EP El Niño events (Gushchina and Dewitte, 2012). In particular, the EP El Niño is characterized by a fast transition from El Niño to La Niña conditions, thus the austral winter circulation anomalies in the mid-to-high latitudes are significantly different from anomalies during austral summer. This results in opposing signs of the lagged regression coefficients of the JJA geopotential onto DJF index (as compare to synchronic regression in austral summer). Noticeably, that simultaneous regression during austral winter displays the same pattern as in austral summer (Figure 6d,f) because towards the austral winter both SST and circulation anomalies change to the opposite of those found during austral summer.

The SH temperature response in austral summer manifests in warmer subtropics except for the Pacific region and south-east of South America (Figure 7a,d). Over Antarctica, the temperature response to CP El Nino events is lacking except for the Western Antarctic. The latter exhibits opposite anomalies associated with the different types of El Niño: positive/negative during EP/CP events. The dipole-like temperature structure is observed over the oceans during both CP and EP El Niño events during austral summer (Figure 7a,d) and is characterized by an opposite sign over the Pacific (positive anomalies to the south and negative to the north) and Atlantic (positive anomalies to the north and negative to the south). In the mid-latitudes of the SH there are no stationary centres of atmosphere comparable to the Iceland and Aleutian lows or the Siberian and Canadian anticyclones in NH. Thus, the positive and negative geopotential anomalies in the SH mid-latitudes are not associated with the intensification or weakening of specific pressure centres but mostly due to the intensification or weakening of cyclonic activity over the Southern Ocean. The intensification (i.e., the negative anomalies) contributes to the negative temperature anomalies due to a reduction in solar radiation and weak cyclonic activity leads to warmer conditions.

The temperature response in austral winter following a CP peak is three times larger than in austral summer, while the spatial structure does not significantly change (Figure 7b,c). The maximum positive anomalies are located over the Pacific and Indian Ocean sectors, while the Weddell Sea and Antarctic Peninsula are characterized by colder conditions. These anomalies may result from the north-westward shift of the anticyclone over Antarctica and associated southern currents over the Weddell Sea and northern currents over the Pacific. The changes in temperature response to EP El Niño from austral summer to winter (Figure 7e,f) are similar to those observed in the geopotential height anomalies at 700 hPa (Figure 6e,f). The lagged regression of austral winter temperature onto the austral summer E index is opposite to the simultaneous regressions in summer and winter over the Eastern Antarctica and EP. However, over Western Antarctica and the Indian and Atlantic Oceans, the lagged regression of austral winter temperature onto the austral summer E index has the same sign as its simultaneous regression counterpart.

We may conclude that the response of the SH circulation does not significantly differ between the two types of El Niño events. It is characterized by an almost symmetric dipole annular structure with positive regression coefficients located in the polar regions surrounded by a belt of negative regression coefficients. In austral summer (winter) it is associated with a weakening (intensifying) circumpolar vortex. An exception is the lagged regression pattern between austral winter circulation anomalies and austral summer E index that is due to the rapid transition

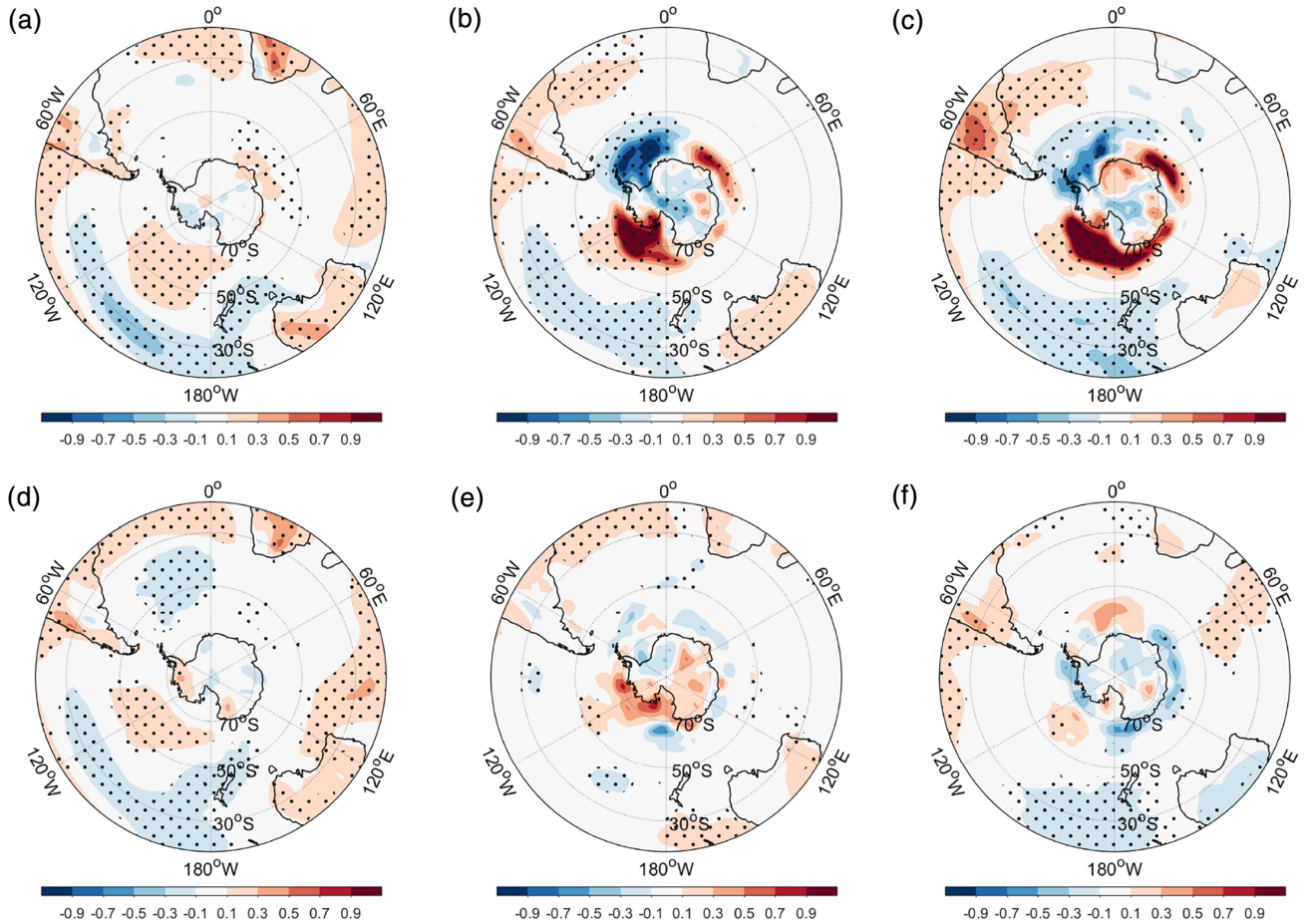

FIGURE 7 Regression of surface air temperature anomalies on C index (a–c): (a) austral summer—austral summer, (b) austral summer—following austral winter, (c) austral winter—austral winter. The first season corresponds to the ENSO index and the second season to temperature anomalies. The same is shown here but for regression on E index (d–f). Contour interval is 0.2°C. The outermost latitude is 20°S [Colour figure can be viewed at wileyonlinelibrary.com]

from El Niño to La Niña that characterizes the evolution of strong EP El Niño events (Santoso *et al*., 2017).

The SH response contrasts with the NH where the difference between CP and EP El Niño events is significant in terms of the ENSO teleconnection. This indicates that ENSO diversity is a source of interhemispheric asymmetry of the ENSO teleconnection.

4 | ENSO TELECONNECTIONS UNDER FUTURE CLIMATE

4.1 | Selection of CMIP5 models

Evolution of the ENSO teleconnection in future climates is uncertain with models exhibiting a weak intermodel agreement from region to region (Yeh *et al*., 2018), but there is more confidence in the evolution of ENSO as projected by these same models (Cai *et al*., 2018). In particular, EP El Niño events are projected to increase in amplitude and frequencies due to both increase in stratification and mean SST (Cai *et al*., 2018; Carréric *et al*., 2020). Increased stratification is also favourable for the increase in amplitude and frequencies of the CP El Niño events (Yeh *et al*., 2009). Because the ENSO teleconnection is nonlinear, which is largely associated with the diversity of El Niño (Frauen *et al*., 2014), subtle changes in the E and C patterns and the mean SST can therefore influence the ENSO teleconnections, explaining the spread in the response of the ENSO teleconnection to global warming in climate models.

Considering the weak intermodel agreement in terms of the ENSO teleconnections (Yeh *et al*., 2018), we select a subgroup of models that not only simulate realistic ENSO diversity but also the AO/AAO mean structure and the teleconnection patterns of geopotential at particular pressure levels associated with the two types of El Niño.

We analysed 17 CMIP5 models that were demonstrated to have skill in simulating ENSO non-linearity

that is a key feature for the model's realism in simulating ENSO diversity (Cai *et al*., 2018). Amongst this subgroup, we select the models that realistically simulate the AO/AAO in the historical runs. The criteria for selecting realistic models was such that models yielding spatial correlation with Reanalysis larger than 80% (90%) for the AO (AAO) were retained.

To evaluate the model's ability to simulate the teleconnection patterns for the two types of El Niño, the comparison between models and Reanalysis was based on spatial correlation (correlation larger than 50 and 40%, respectively, for the NH and SH) of the regression of geopotential at 925 hPa in the NH (the data for 1,000 hPa is not available for several models) and at 500 hPa in the SH onto the E and C indices. The regression patterns for 500 and 700 hPa are similar in SH but at 500 hPa there are fewer data gaps because of topography. The different threshold for correlation between the SH and NH is due to the fact that only 1 model amongst the 17 yielded a value for correlation higher than 50% during austral winter in the SH. These rather stringent criteria yields the selection of 5 CMIP5 models for the NH (CMCC-CMS, GISS-E2-R, FIO-ESM, CESM1-CAM5 and IPSL-CM5B-LR), 8 models for the SH in austral summer (bbc-csm1-1-m, CCSM4, CESM1-BGC, CESM1-CAM5, CNRM-CM5, FIO-ESM, GFDL-ESM2M and MIROC5) and 5 models in SH in austral winter (CCSM4, CESM1-CAM5, CNRM-CM5, GFDL-ESM2M and MIROC5). In the following, the results are presented as the ensemble mean of the selected CMIP5 models.

4.2 | RESULTS

4.2.1 | Geopotential

The regression coefficients of geopotential at 925 (500) hPa for the NH (SH) onto the E and C indices for the historical and RCP8.5 experiments, along with their differences, are presented (Figures 8 and 9). Since the seasonal ENSO variance changes in the warmer climate, in order to objectively compare the regression maps for the RCP8.5 and historical scenario, the regression coefficients for RCP8.5 were scaled with the coefficient $\frac{rms(E_{rcp})}{rms(E_{hist})}$ and $\frac{rms(C_{rcp})}{rms(C_{hist})}$ for EP and CP El Niño respectively. The subscript refers to the scenario (RCP8.5 vs. historical) of a selected model, and we consider the DJF mean for the E and the C timeseries so that their root mean square (rms) is not necessarily equal to unity. Note that during DJF, the variance in E and C indices exhibits an increase in the warmer climate on the order of ∼15% (Cai *et al*., 2018). The results indicate that the spatial structure of planetary circulation response to both types of El Niño events does not significantly change from the present to the future climate. In the NH, the AO-like response to CP events and the wave-like response to EP events clearly manifest (Figure 8). In the SH, the annular geopotential structure is observed in both climates (Figure 9). However, the amplitude of the regression coefficient is significantly increased in some regions in the warmer climate. For instance, over the North Pacific, the negative coefficient value increases by 30% from the present to the warmer climate, which corresponds to an increased intensity of the Aleutian low. Over the NH polar region, the amplitude increased by 25%, which corresponds to a weakening of the circumpolar vortex. For both hemispheres, the difference between the RCP8.5 and historical experiments can be interpreted as an overall intensification of the circulation response to ENSO during boreal winter (Figures 8 and 9 right columns) although the intensification is less evident in the SH. The latter is mostly due to the weak inter-model agreement: three models (CESM1-CAM5, CNRM-CM5 and MIROC5) simulate a weaker CP event teleconnection and 5 models (CCSM4, CESM1-BGC, CNRM-CM5, bbc-csm1-1-m and GFDL-ESM2M) simulate weaker EP event teleconnections in the SH in the warmer climate. The intensification of the circulation response is observed both in the low (925 hPa) and middle (500 hPa) troposphere (not shown for NH).

In austral winter, we may observe the similar amplification tendency; the averaged regression coefficient values in the main anomaly centres increased by 20–25% in the warmer climate (Figure 10i,l). However, the strongest intensification of the SH response to ENSO in the future climate manifests in the circulation anomalies in austral winter regressed onto the austral summer El Niño indices (Figure 10c,f), indicating that increase in El Niño variance may induce an increase in the austral winter southern circumpolar vortex amplitude in the warmer climate. The latter in turn may yield stronger isolation of Antarctic atmosphere and depletion of the ozone layer as intense circumpolar circulation prevents warmer and ozone-rich air masses from the mid-latitudes to penetrate into the Antarctic (Solomon *et al*., 2014).

4.2.2 | Surface air temperature

The regression coefficients of air temperature onto the E and C indices in the NH for present and future climates and their differences are presented (Figure 11). It evidences the amplification of positive temperature

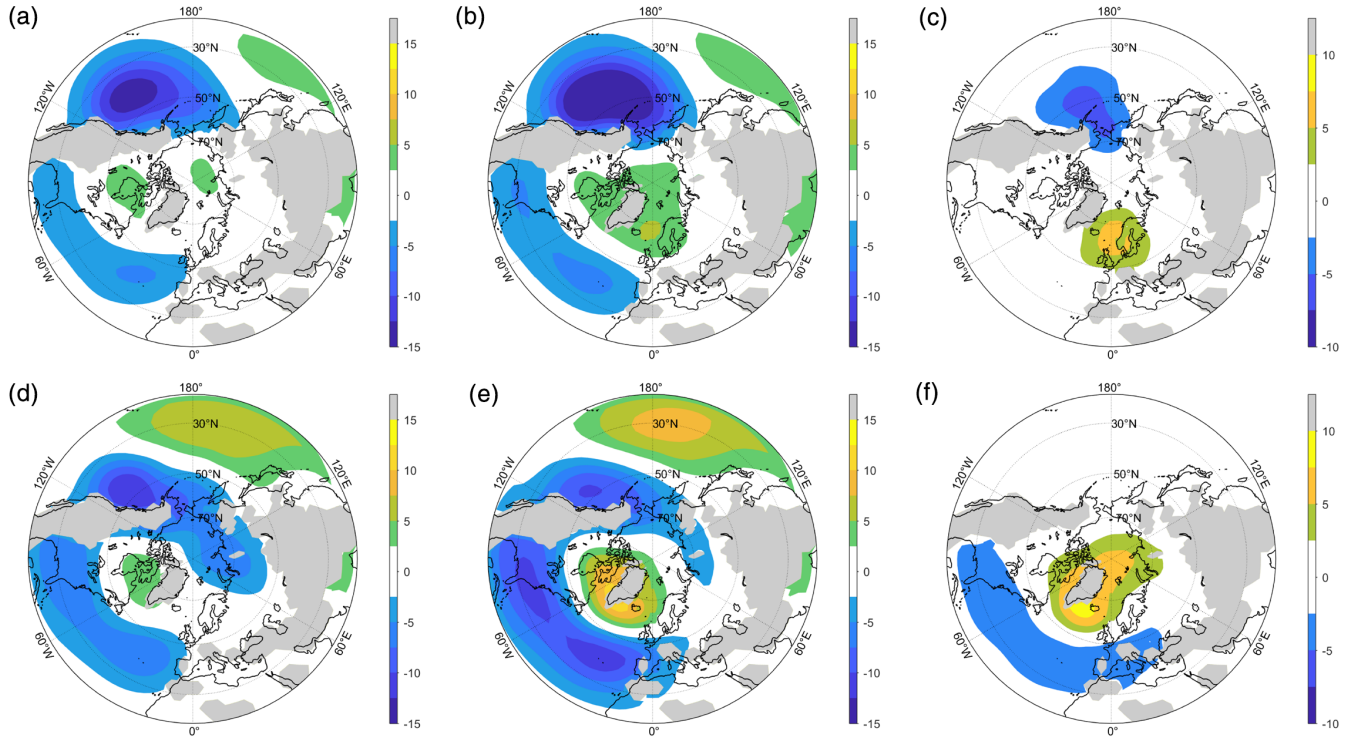

FIGURE 8 Averaged CMIP5 model (see the text) regression of geopotential height anomalies at 925 hPa level in boreal winter on C index for (a) 1916–2005 period (historical run), (b) 2006–2095 period (RCP8.5 experiment) and (c) differences between RCP8.5 and historical runs. The same is shown here but for regression on E index (d–f). The regression coefficients for RCP8.5 are normalized by $\frac{rms(E_{rcp})}{rms(E_{hist})}$ and $\frac{rms(C_{rcp})}{rms(C_{hist})}$ for EP and CP El Niño, respectively, where the subscript refers to the scenario (RCP8.5 vs. historical) and rms refers to the root mean square. Contour interval is 2.5 hPa. The outermost latitude is 20°N [Colour figure can be viewed at wileyonlinelibrary.com]

anomalies associated with the CP events over the Canadian and central sector of the Arctic, while also highlighting that the negative anomalies over the Pacific hardly change in amplitude or peak location. This is consistent with the changes in circulation discussed above (intensification/weakening of Aleutian low/circumpolar vortex). However, the change of the temperature response in warmer climate is not uniform: strong on the eastern periphery of the Aleutian low (positive anomalies due to advection of warm air) and weak on the western periphery (negative anomalies associated to cold advection from high latitudes). This could be due to the nonlinear amplification of the temperature response over the continent and rectification processes associated with the absorption of solar radiation enhanced by the snowmelt-albedo feedback (Jakobs *et al.*, 2019) or the effect of snow cover and type of precipitation (snow vs. rain) onto boundary layer dynamics. This apparent inconsistency between the circulation and temperature climate change patterns calls for further investigation, which is beyond the scope of this paper.

The most prominent amplification of temperature response in future climate is observed over Alaska during CP events (Figure 11c); in particular, the warming associated with CP El Niño events is three times larger in the future climate than in the present climate. This larger sensitivity of air-temperature anomalies to CP El Niño events in the warmer climate may exacerbate the strong positive temperature trend in the Arctic through rectification processes. These non-linear processes could include the seasonal recovery of sea ice extent in the Arctic during CP El Niño years that would impact air temperature through ice-air interactions, or changes in ocean mixing associated with anomalous weather conditions during CP El Niño years. The amplification of temperature response to CP El Niño over Eurasia is less clear, possibly due to biases in some models. In particular, the models FIO-ESM and IPSL-CM5B-LR simulate positive temperature anomalies over Eurasia in the present climate whereas the Reanalysis indicates that a CP El Niño event yields cooling in this region (Figure 4a). The amplification of temperature anomalies associated with EP El Niño events in the future climate is less pronounced compared to CP El Niño events, reflecting weaker inter-model consensus (Figure 11f). Meanwhile, the intensification of positive temperature anomalies manifests over Greenland, Arctic Ocean, Kamchatka, the Okhotsk Sea and Western Siberia. The cooling associated with EP events amplifies over

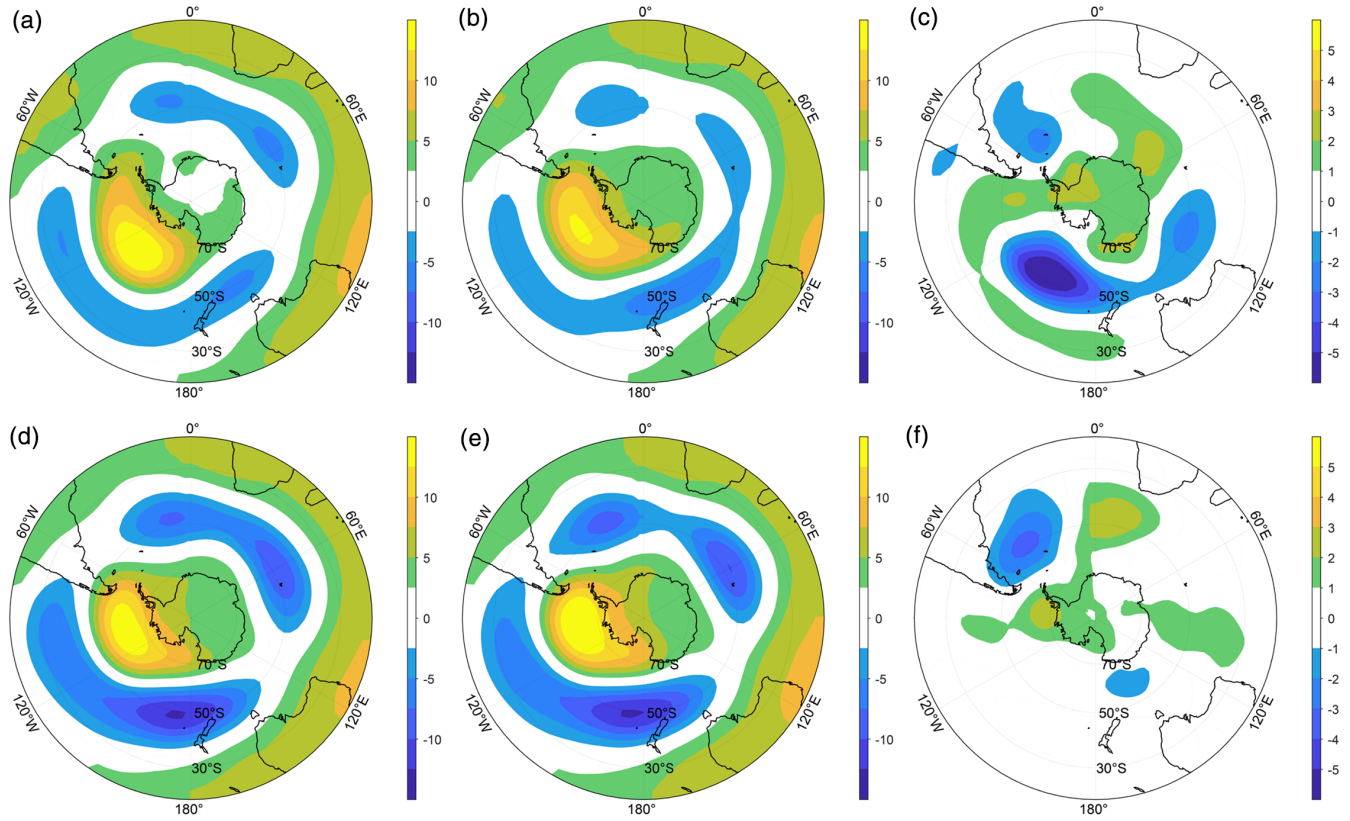

FIGURE 9 Averaged CMIP5 model regression of geopotential height anomalies at 500 hPa level in austral summer on C index for (a) 1916–2005 period (historical run), (b) 2006–2095 period (RCP8.5 experiment) and (c) difference between RCP8.5 and historical runs. The same is shown here but for regression on E index (d–f). The regression coefficients for RCP8.5 are normalized by $\frac{rms(E_{rcp})}{rms(E_{hist})}$ and $\frac{rms(C_{rcp})}{rms(C_{hist})}$ for EP and CP El Niño, respectively, where the subscript refers to the scenario (RCP8.5 vs. historical) and rms refers to the root mean square. Contour interval is 2.5 hPa in panels (a,b,d,e) and 1 hPa in panels (c,f). The outermost latitude is 20°S [Colour figure can be viewed at wileyonlinelibrary.com]

the mid and subtropical latitudes of Northern America (Figure 11f).

In the SH, the temperature response in DJF to both types of El Niño is weaker compared to the NH and the changes associated with global warming are not pronounced (Figure 12c,f). In austral winter, the temperature response to El Niño weakens in the future climate both for simultaneous and lagged regressions (Figure 12i,l,o,r).

5 | DISCUSSION AND CONCLUSIONS

In this article, we investigated the atmospheric teleconnections in the mid-to-high latitudes associated with the different types of El Niño events, complementing previous studies (reviewed in Yeh *et al.*, 2018; Cai *et al.*, 2019, 2020). Our focus was on the relationship between modes of variability in the high-latitudes (i.e., AO and AAO) and the ENSO teleconnection patterns, considering that their interactions may yield significant climate extremes and exacerbate long-term trends (e.g., Stuecker *et al.*, 2017) and that there is a low-frequency modulation of ENSO diversity. We show that, in the NH in DJF, the CP El Niño events that have become more frequent since the 1990s, induce a negative AO-like circulation pattern. In the SH in DJF, however, the ENSO teleconnection patterns are comparable to the negative AAO circulation pattern for both types of El Niño. Thus, while there is a significant difference between the DJF circulation response to CP and EP events in the NH, this is not the case for the SH.

In the SH the main difference between the circulation response to CP and EP events consists in persistence of the response. During EP El Niño the composite circulation anomalies change significantly from austral summer to winter with an anomalous circulation pattern similar to that of the negative (positive) phase of AAO in austral summer (winter), while the composite circulation anomalies during CP El Niño hardly change from DJF to JJA. This could result from the fast transition from warm to

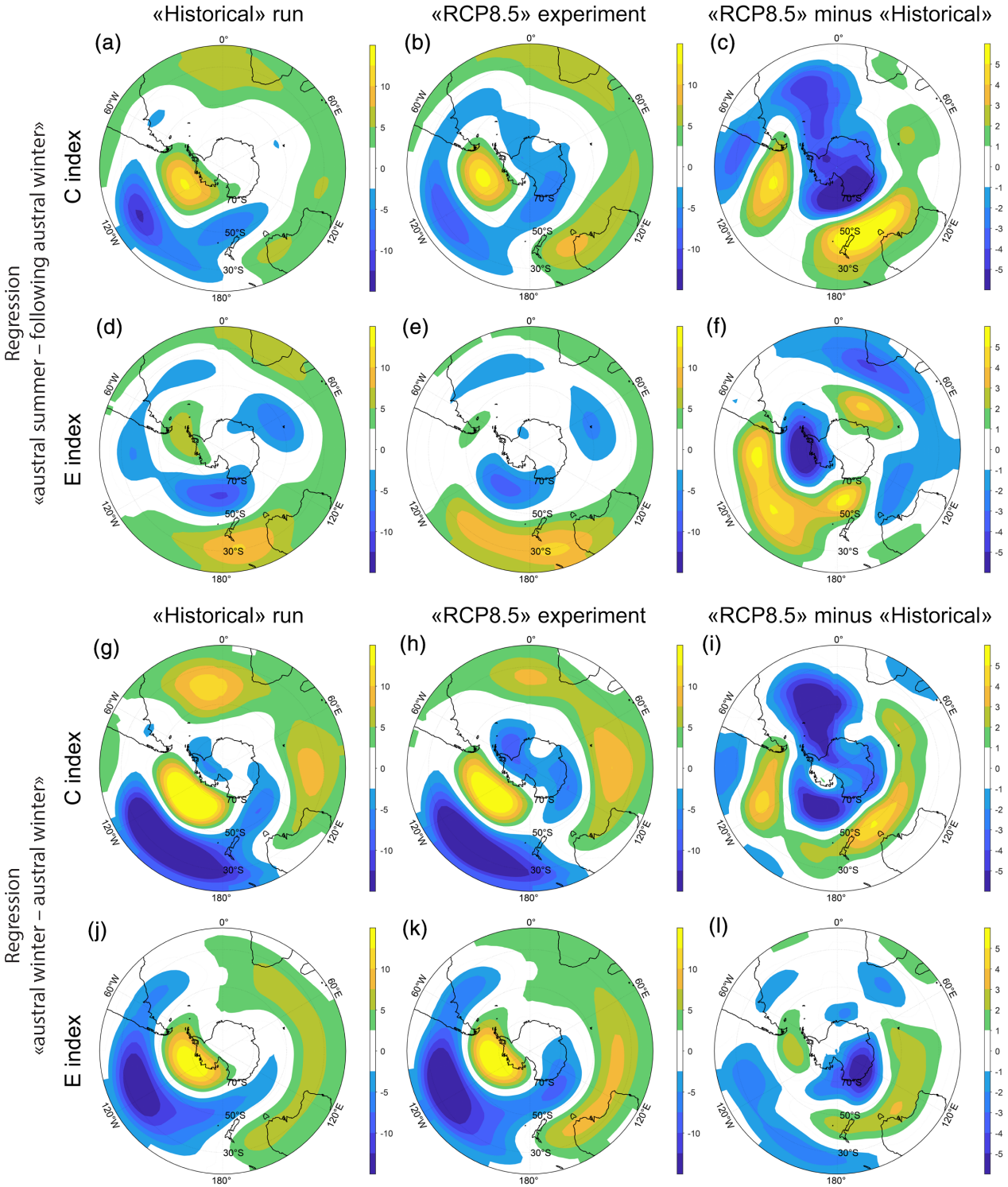

FIGURE 10 Averaged CMIP5 model regression of geopotential height anomalies at 500 hPa level on ENSO indices for 1916–2005 period—historical run (first column), 2006–2095 period—RCP8.5 experiment (second column) and difference between RCP8.5 and historical runs (third column) for (a–f) austral summer—following austral winter, (g–l) austral winter—austral winter. The first season corresponds to ENSO index; the second season—to geopotential anomalies. The top panel is regression on C index, the bottom—on E index. The regression coefficients for RCP8.5 are normalized by $\frac{rms(E_{rcp})}{rms(E_{hist})}$ and $\frac{rms(C_{rcp})}{rms(C_{hist})}$ for EP and CP El Niño, respectively, where the subscript refers to the scenario (RCP8.5 vs. historical) and rms refers to the root mean square. Contour interval is 2.5 hPa in panels (a,b,d,e,g,h,j,k) and 1 hPa in panels (c,f,i,l). The outermost latitude is 20°S [Colour figure can be viewed at wileyonlinelibrary.com]

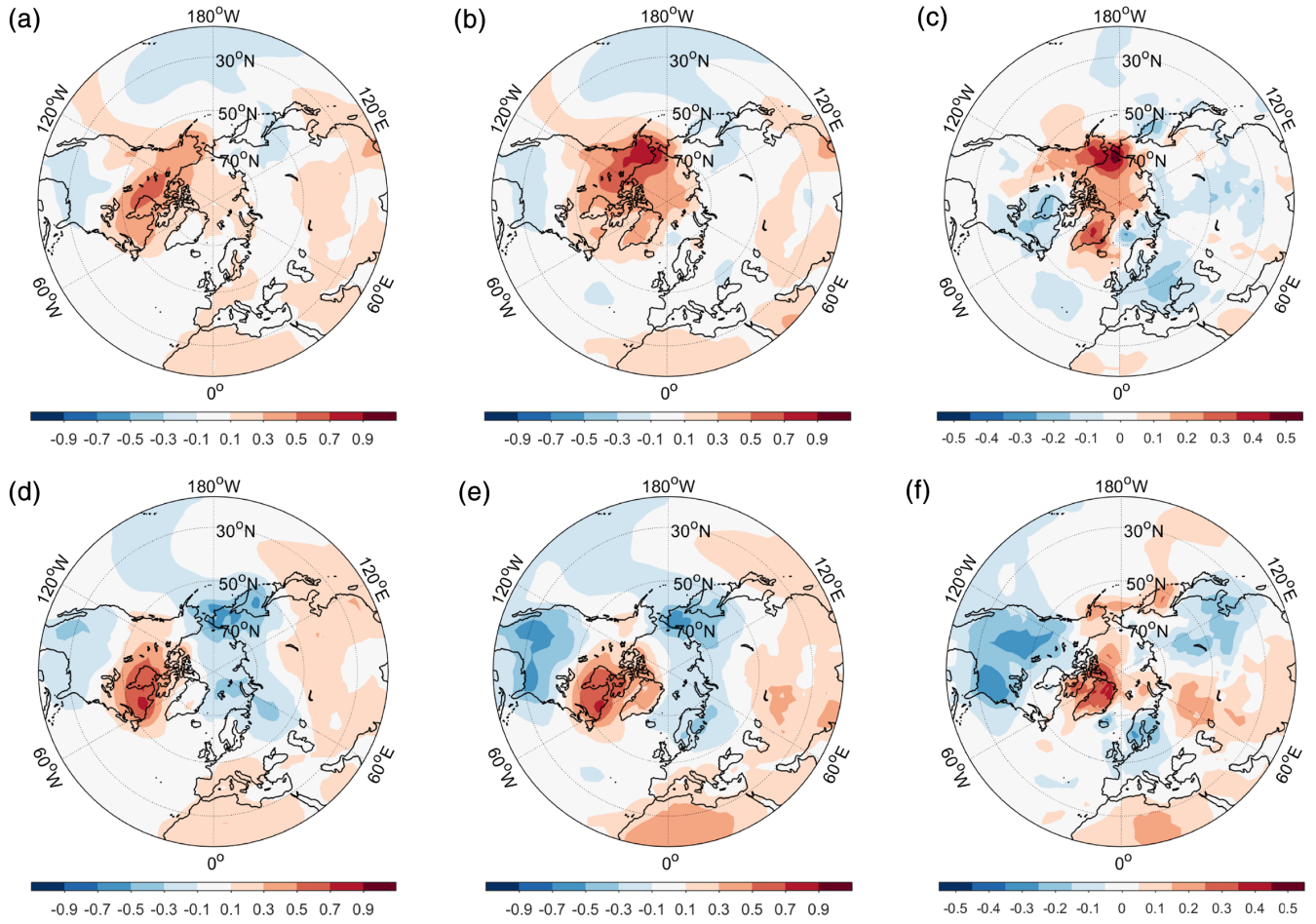

FIGURE 11 Averaged CMIP5 model regression of surface air temperature anomalies in boreal winter on C index for (a) 1916–2005 period (historical run), (b) 2006–2095 period (RCP8.5 experiment) and (c) difference between RCP8.5 and historical runs. The same is shown here but for regression on E index (d–f). The regression coefficients for RCP8.5 are normalized by $\frac{rms(E_{rcp})}{rms(E_{hist})}$ and $\frac{rms(C_{rcp})}{rms(C_{hist})}$ for EP and CP El Niño, respectively, where the subscript refers to the scenario (RCP8.5 vs. historical) and rms refers to the root mean square. Contour interval is 0.2°C in panels (a,b,d,e) and 0.1°C in panels (c,f). The outermost latitude is 20°N [Colour figure can be viewed at wileyonlinelibrary.com]

cold tropical Pacific SST anomalies in austral autumn (MJJ) during strong EP El Niño events, while CP El Niño SST anomalies have a longer persistence (Dewitte *et al*., 2012).

This implies that there is an interhemispheric asymmetry of the ENSO teleconnection associated with ENSO diversity. In the NH in boreal winter during EP events, the Rossby wave emanating poleward and arching eastward induces circulation anomalies confined to the Pacific region in the low troposphere (1,000 hPa) and the wave structure with zonal wavenumber 3 in the middle troposphere (500 hPa). During such events in the SH, the atmospheric response consists of an approximately symmetric dipole annular structure, similar to what occurs during CP El Niño events. Previous studies have emphasized the non-linearity of the ENSO teleconnection associated with ENSO diversity (Cai *et al*., 2010; Frauen *et al*., 2004). Here, we suggest that such non-linearity contributes to the interhemispheric asymmetry of the ENSO teleconnection to the high-latitudes. Given an El Niño SST spatial pattern, interhemispheric asymmetry of the ENSO teleconnection is expected due to the interhemispheric asymmetry of the mean atmospheric circulation and the existence of two main distinct mechanisms of teleconnection sensitive to the mean state (i.e., the wave train mechanism and eddy-jet mechanism; reviewed in Yang *et al*., 2018)). We argue here that ENSO diversity reinforces this interhemispheric asymmetry because the ENSO teleconnection is more sensitive to the El Niño types in the NH than over the SH.

Such interhemispheric asymmetry is also observed in the response of surface air-temperature anomalies. Over most of the NH, the temperature regression patterns are almost opposite for CP/EP events and the temperature response to CP events is similar to the temperature anomalies associated with the negative AO phase. The pattern of the temperature response to El Niño in the SH,

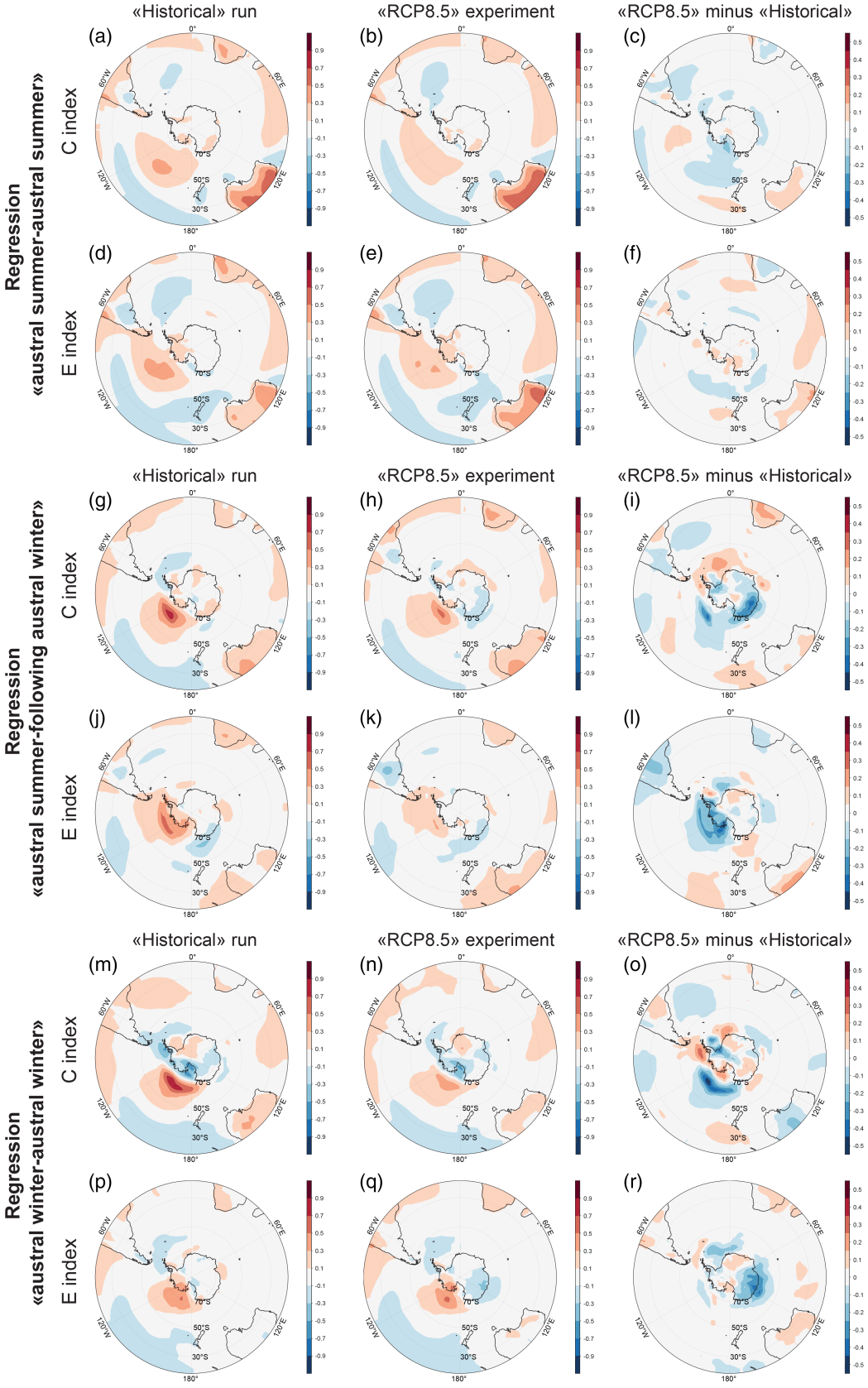

FIGURE 12 Legend on next page.

however, is comparable for both types of El Niño events and deviates slightly from that of the AAO along with exhibiting marked seasonal variations (i.e., it is three times larger in austral winter than in summer).

Limitation of our study includes the fact that reanalysis products correspond to one realization of the climate variability, so that internal atmospheric variability may contribute to emphasizing the ENSO teleconnection pattern inferred from the reanalysis (Langenbrunner and Neelin, 2013). To estimate the relative contribution of internal atmospheric variability versus the ENSO forced signal, we take advantage of the ERA-20CM atmospheric simulations performed at the European Centre for Medium-Range Weather Forecasts (ECMWF) that provides 10 simulations for the period 1900–2010 (Hersbach *et al*., 2015). The 10 simulations allow an estimate of internal atmospheric dynamics through the inspection of dispersion amongst the ensemble. We performed a similar analysis to that of Figure 1c,d but using the 10 members of ERA-20CM for the period 1950–2010, which corresponds to the overlapping period with that used for the analysis of the NCEP-NCAR Reanalysis (Figure S2). The results indicate that there is significant dispersion in the ENSO teleconnections patterns in the high-latitudes (less so in the mid-latitudes) in this model, suggesting that internal atmospheric variability may be significant in the atmospheric response to ENSO. In particular, the structure of the circulation response to both types of El Niño in ERA-20CM is similar to the PNA pattern (Figures S2b,e), while the AO-like negative phase structure is not observed in the ERA-20CM ensemble mean for the C pattern (Figure S2e) as compare to NCEP-NCAR (Figure S2a).

Thus, from the analysis of ERA-20CM, we cannot rule out the hypothesis that our results based on NCEP-NCAR could be partly explained by natural variability rather than by ENSO. However, there is the possibility that the magnitude of the dispersion is overestimated in ERA-20CM due to either model bias or the limited numbers of ensemble members. In particular, biases in the mean circulation can energize the eddy flux and yield unrealistic simulations of the internal atmospheric variability. The experimental design of the AMIP run also has the limitation of not taking into account explicitly regional air-sea-land interactions processes that could also be important for modulating the ENSO teleconnections. Further studies based on larger ensembles is thus required to quantitatively determine the magnitude of internal dynamics in modulating the forced response to ENSO in the high-latitudes.

With this limitation in mind, we have analysed models participating to CMIP5 focusing on those that realistically simulate both ENSO diversity and the high-latitude climate modes (i.e., AO and AAO). We showed that, in the warmer climate, there is an amplification of the circulation response for both types of El Niño and in both hemispheres, that is, the circulation anomalies in the mid-to-high latitudes are stronger in the warmer than in the modern climate, while the amplitude of El Niño events does not significantly changed. However, the spatial pattern (spatial structure) of the response is unchanged. The reasons for increased sensitivity of the atmospheric response in the high-latitudes to ENSO remain to be addressed. At this stage, it is interesting to note that our model ensemble does not exhibit significant changes in the patterns of ENSO in the warmer climate (not shown), so it is likely that such amplification results from changes in mean state, whether in the tropical regions or/and in the extra-tropics, that would favour the mechanisms mentioned above. This issue deserves further investigation that is beyond the scope of the present study. Furthermore, amplification of the ENSO teleconnections in the warmer climate manifests in the surface temperature fields, mostly in the NH and for the CP El Niño events. The positive temperature anomalies in the NH polar regions (especially over Alaska) associated with CP El Niño teleconnection may amplify the overall warming trend in the high-latitudes through non-linear (rectification) processes, and in particular in the Arctic region. Considering the serious climatic implications of such scenario, our results call for investigating the interaction between ENSO-induced variability and long-term trends over the Arctic region in order to assess if the ENSO teleconnection can exacerbate or mitigate the current warming trend in this region.

ACKNOWLEDGEMENTS

D. Gushchina and M. Kolennikova acknowledge support from the Russian Scientific Foundation (RFS), project 19-17-00198. B. Dewitte acknowledges support from ANID (Concurso de Fortalecimiento al Desarrollo Científico de

FIGURE 12 Averaged CMIP5 model regression of surface air temperature anomalies on ENSO indices for 1916–2005 period—historical run (first column), 2006–2095 period—RCP8.5 experiment (second column) and difference between RCP8.5 and historical runs (third column) for (a–f) austral summer—austral summer, (g–l) austral summer—following austral winter, (m–r) austral winter—austral winter. The first season corresponds to ENSO index and the second season to temperature anomalies. The top panel is regression on C index, the bottom on E index. The regression coefficients for RCP8.5 are normalized by $\frac{rms(E_{rcp})}{rms(E_{hist})}$ and $\frac{rms(C_{rcp})}{rms(C_{hist})}$ for EP and CP El Niño, respectively, where the subscript refers to the scenario (RCP8.5 vs. historical) and rms refers to the root mean square. Contour interval is 0.2°C in panels (a,b,d, e,g,h,j,k,m,n,p,q) and 0.1°C in panels (c,f,i,l,o,r). The outermost latitude is 20°S [Colour figure can be viewed at wileyonlinelibrary.com]

Centros Regionales 2020-R20F0008-CEAZA and Grant 1190276) and ANR (Grant ANR-18-CE01-0012). S.W. Yeh was funded by the Korean Meteorological Administration Research and Development Program under grant (KMI2020-01213). The authors acknowledge EcoSpatial Services L.L.C. (USA) for the English language editing.

AUTHOR CONTRIBUTIONS

Daria Gushchina: Conceptualization; investigation; methodology; supervision; writing - original draft; writing-review & editing. **Maria Kolennikova:** Formal analysis; investigation; software; visualization; writing - original draft. **Boris Dewitte:** Conceptualization; methodology; writing - original draft; writing-review & editing. **Sang-Wook Yeh:** Writing-review & editing.

ORCID

Daria Gushchina https://orcid.org/0000-0002-9892-2040

Sang-Wook Yeh https://orcid.org/0000-0003-4549-1686

REFERENCES

Ambrizzi, T. and Hoskins, B.J. (1997) Stationary rossby-wave propagation in a baroclinic atmosphere. *Quarterly Journal Royal Meteorological Society*, 123, 919–928. https://doi.org/10.1002/qj.49712354007.

Ashok, K., Behera, S.K., Rao, S.A., Weng, H. and Yamagata, T. (2007) El Niño Modoki and its possible teleconnection. *Journal of Geophysical Research*, 112, C11007. https://doi.org/10.1029/2006JC003798.

Ayarzagüena, B., Ineson, S., Dunstone, N.J., Baldwin, M.P. and Scaife, A.A. (2018) Intraseasonal Effects of El Niño–Southern Oscillation on North Atlantic Climate. *Journal of Climate*, 31(21), 8861–8873. https://doi.org/10.1175/jcli-d-18-0097.1.

Baldwin, M.P., Birner, T., Brasseur, G., Burrows, J., Butchart, N., Garcia, R., Geller, M., Gray, L., Hamilton, K., Harnik, N., Hegglin, M.I., Langematz, U., Robock, A. and Sato, K. (2019) 100 years of progress in understanding the stratosphere and mesosphere. *Meteorological Monographs*, 59, 27.1–27.62. https://doi.org/10.1175/AMSMONOGRAPHS-D-19-0003.1.

Brands, S. (2017) Which ENSO teleconnections are robust to internal atmospheric variability? *Geophysical Research Letters*, 44, 1483–1493. https://doi.org/10.1002/2016GL071529.

Branstator, G. (2002) Circumglobal teleconnections, the jet stream waveguide, and the North Atlantic oscillation. *Journal of Climate*, 15(14), 1893–1910.

Cai, W., McPhaden, M.J., Grimm, A.M., Rodrigues, R., Taschetto, A.S., Garreaud, R., Dewitte, B., Poveda, G., Ham, Y.-G., Santoso, A., Ng, B., Anderson, W., Wang, G., Geng, T., Jo, H.-S., Marengo, J., Alves, L.M., Osman, M., Li, S., Wu, L., Karamperidou, C., Takahashi, K. and Vera, C. (2020) Climate impacts of the El Niño–Southern Oscillation on South America. *Nature Reviews Earth & Environment*, 1, 215–231.

Cai, W., van Rensch, P., Cowan, T. and Sullivan, A. (2010) Asymmetry in ENSO Teleconnection with Regional Rainfall, Its Multidecadal Variability, and Impact. *Journal of Climate*, 23(18), 4944–4955. https://doi.org/10.1175/2010JCLI3501.1.

Cai, W., Wang, G., Dewitte, B., Wu, L., Santoso, A., Takahashi, K., Yang, Y., Carréric, A. and McPhaden, M.J. (2018) Increased variability of eastern Pacific El Niño under greenhouse warming. *Nature*, 564, 201–206. https://doi.org/10.1038/s41586-018-0776-9.

Cai, W., Wu, L., Lengaigne, M., Li, T., McGregor, S., Kug, J.-S., Yu, J.-Y., Stuecker, M.F., Santoso, A., Li, X., Ham, Y.-G., Chikamoto, Y., Ng, B., McPhaden, M.J., Du, Y., Dommenget, D., Jia, F., Kajtar, J.B., Keenlyside, N., Lin, X., Luo, J.-J., Martín-Rey, M., Ruprich-Robert, Y., Wang, G., Xie, S.-P., Yang, Y., Kang, S.M., Choi, J.-Y., Gan, B., Kim, G.-I., Kim, C.-E., Kim, S., Kim, J.-H. and Chang, P. (2019) Pantropical climate interactions. *Science*, 363(6430), eaav4236. https://doi.org/10.1126/science.aav4236.

Capotondi, A., Wittenberg, A.T., Newman, M., Di Lorenzo, E., Yu, J.Y., Braconnot, P., Cole, J., Dewitte, B., Giese, B., Guilyardi, E., Jin, F.F., Karnauskas, K., Kirtman, B., Lee, T., Schneider, N., Xue, Y. and Yeh, S.W. (2015) Understanding ENSO diversity. *Bulletin of the American Meteorological Society*, 96(6), 921–938. https://doi.org/10.1175/BAMS-D-13-00117.1.

Carréric, A., Dewitte, B., Cai, W., Capotondi, A., Takahashi, K., Yeh, S.-W., Wang, G. and Guémas, V. (2020) Change in strong Eastern Pacific El Niño events dynamics in the warming climate. *Climate Dynamics*, 54, 901–918. https://doi.org/10.1007/s00382-019-05036-0.

Carvalho, L.M.V., Jones, C. and Ambrizzi, T. (2005) Opposite Phases of the Antarctic Oscillation and Relationships with Intraseasonal to Interannual Activity in the Tropics during the Austral Summer. *Journal of Climate*, 18(5), 702–718. https://doi.org/10.1175/JCLI-3284.1.

Ciasto, L.M. and Thompson, D.W.J. (2008) Observations of Large-Scale Ocean–Atmosphere Interaction in the Southern Hemisphere. *Journal of Climate*, 21(6), 1244–1259. https://doi.org/10.1175/2007JCLI1809.1.

Dee, D.P., Uppala, S.M., Simmons, A.J., Berrisford, P., Poli, P., Kobayashi, S., Andrae, U., Balmaseda, M.A., Balsamo, G., Bauer, P., Bechtold, P., Beljaars, A.C.M., van de Berg, L., Bidlot, J., Bormann, N., Delsol, C., Dragani, R., Fuentes, M., Geer, A.J., Haimberger, L., Healy, S.B., Hersbach, H., Hólm, E. V., Isaksen, L., Kållberg, P., Köhler, M., Matricardi, M., McNally, A.P., Monge-Sanz, B.M., Morcrette, J.-J., Park, B.-K., Peubey, C., de Rosnay, P., Tavolato, C., Thépaut, J.-N. and Vitart, F. (2011) The ERA-Interim reanalysis: configuration and performance of the data assimilation system. *Quarterly Journal of the Royal Meteorological Society*, 137(656), 553–597. https://doi.org/10.1002/qj.828.

Dewitte, B., Choi, J., An, S.-I. and Thual, S. (2012) Vertical structure variability and equatorial waves during central Pacific and eastern Pacific El Niños in a coupled general circulation model. *Climate Dynamics*, 38, 2275–2289. https://doi.org/10.1007/s00382-011-1215-x.

Dewitte, B. and Takahashi, K. (2019) Extreme El Niño events. In: Venugopal, V., Sukhatme, J., Murtugudde, R. and Roca, R. (Eds.) *Tropical Extremes: Natural Variability and Trends*. Amsterdam: Elsevier, 165–201. https://doi.org/10.1016/B978-0-12-809248-4.00006-6.

Di Lorenzo, E., Cobb, K.E., Furtado, J.C., Schneider, N., Anderson, B., Bracco, A., Alexander, M. and Vimont, D. (2010) Central Pacific El Niño and decadal climate change in the North Pacific Ocean. *Nature Geoscience*, 3, 762–765.

Ding, H., Greatbatch, R.J., Lin, H., Hansen, F., Gollan, G. and Jung, T. (2016) Austral winter external and internal atmospheric variability between 1980 and 2014. *Geophysical Research Letters*, 43(5), 2234–2239.

Ding, Q., Steig, E.J., Battisti, D.S. and Wallace, J.M. (2012) Influence of the Tropics on the Southern Annular Mode. *Journal of Climate*, 25(18), 6330–6348.

Dommenget, D. and Yu, Y. (2017) The effects of remote SST forcings on ENSO dynamics, variability and diversity. *Climate Dynamics*. 49(7-8), 2605–2624. https://doi.org/10.1007/s00382-016-3472-1.

Drouard, M., Rivière, G. and Arbogast, P. (2013) The North Atlantic Oscillation Response to Large-Scale Atmospheric Anomalies in the Northeastern Pacific. *Journal of the Atmospheric Sciences*, 70(9), 2854–2874. https://doi.org/10.1175/JAS-D-12-0351.1.

Fogt, R.L. and Bromwich, D.H. (2006) Decadal Variability of the ENSO Teleconnection to the High-Latitude South Pacific Governed by Coupling with the Southern Annular Mode*. *Journal of Climate*, 19(6), 979–997. https://doi.org/10.1175/jcli3671.1.

Frauen, C., Dommenget, D., Tyrrell, N., Rezny, M. and Wales, S. (2014) Analysis of the Nonlinearity of El Niño–Southern Oscillation Teleconnections. *Journal of Climate*, 27(16), 6225–6244.

Graf, H.-F. and Zanchettin, D. (2012) Central Pacific El Niño, the "subtropical bridge," and Eurasian climate. *Journal of Geophysical Research*, 117, D01102. https://doi.org/10.1029/2011JD016493.

Grassi, B., Redaelli, G. and Visconti, G. (2005) Simulation of polar Antarctic trends: influence of tropical SST. *Geophysical Research Letters*, 32(23).

Gushchina, D. and Dewitte, B. (2012) Intraseasonal tropical atmospheric variability associated with the two flavors of El Niño. *Monthly Weather Review*, 140(11), 3669–3681. https://doi.org/10.1175/MWR-D-11-00267.1.

Hersbach, H., Peubey, C., Simmons, A., Berrisford, P., Poli, P. and Dee, D. (2015) ERA-20CM: a twentieth-century atmospheric model ensemble. *Quarterly Journal of the Royal Meteorological Society*, 141, 2350–2375. https://doi.org/10.1002/qj.2528.

Horel, J.D. and Wallace, J.M. (1981) Planetary-Scale Atmospheric Phenomena Associated with the Southern Oscillation. *Monthly Weather Review*, 109(4), 813–829. https://doi.org/10.1175/1520-0493(1981)109<0813:PSAPAW>2.0.CO;2.

Hoskins, B.J. and Karoly, D.J. (1981) The Steady Linear Response of a Spherical Atmosphere to Thermal and Orographic Forcing. *Journal of the Atmospheric Sciences*, 38(6), 1179–1196. https://doi.org/10.1175/1520-0469(1981)038<1179:TSLROA>2.0.CO;2.

Jakobs, C.L., Reijmer, C.H., Kuipers Munneke, P., König-Langlo, G. and van den Broeke, M.R. (2019) Quantifying the snowmelt–albedo feedback at Neumayer Station, East Antarctica. *The Cryosphere*, 13, 1473–1485. https://doi.org/10.5194/tc-13-1473-2019.

Jia, X., Lin, H. and Derome, J. (2009) The influence of tropical Pacific forcing on the Arctic Oscillation. *Climate Dynamics*, 32, 495–509.

Jiménez-Esteve, B. and Domeisen, D.I.V. (2018) The Tropospheric Pathway of the ENSO–North Atlantic Teleconnection. *Journal of Climate*, 31(11), 4563–4584. https://doi.org/10.1175/JCLI-D-17-0716.1.

Kalnay, E., Kanamitsu, M., Kistler, R., Collins, W., Deaven, D., Gandin, L., Iredell, M., Saha, S., White, G., Woollen, J., Zhu, Y., Chelliah, M., Ebisuzaki, W., Higgins, W., Janowiak, J., Mo, K. C., Ropelewski, C., Wang, J., Leetmaa, A., Reynolds, R., Jenne, R. and Joseph, D. (1996) The NCEP/NCAR 40-year reanalysis project. *Bulletin of the American Meteorological Society*, 77, 437–471.

Kao, H.-Y. and Yu, J.-Y. (2009) Contrasting Eastern-Pacific and Central-Pacific Types of ENSO. *Journal of Climate*, 22(3), 615–632. https://doi.org/10.1175/2008JCLI2309.1.

Karamperidou, C., Jin, F.F. and Conroy, J.L. (2017) The importance of ENSO nonlinearities in tropical pacific response to external forcing. *Climate Dynamics*, 49, 2695–2704. https://doi.org/10.1007/s00382-016-3475-y.

Karoly, D.J. (1989) Southern Hemisphere Circulation Features Associated with El Niño-Southern Oscillation Events. *Journal of Climate*, 2(11), 1239–1252. https://doi.org/10.1175/1520-0442(1989)002<1239:SHCFAW>2.0.CO;2.

Kryjov, V.N. and Park, C.-K. (2007) Solar modulation of the El Niño/Southern Oscillation impact on the northern hemisphere annular mode. *Geophysical Research Letters*, 34, L10701. https://doi.org/10.1029/2006GL028015.

Kryzhov, V.N. and Gorelits, O.V. (2015) The Arctic Oscillation and its impact on temperature and precipitation in Northern Eurasia in the 20th Century. *Russian Meteorology and Hydrology*, 40, 711–721. https://doi.org/10.3103/S1068373915110011.

Kug, J.S., Jin, F.F. and An, S.I. (2009) Two Types of El Niño Events: Cold Tongue El Niño and Warm Pool El Niño. *Journal of Climate*, 22(6), 1499–1515. https://doi.org/10.1175/2008JCLI2624.1.

L'Heureux, M.L. and Thompson, D.W.J. (2006) Observed Relationships between the El Niño–Southern Oscillation and the Extratropical Zonal-Mean Circulation. *Journal of Climate*, 19(2), 276–287. https://doi.org/10.1175/JCLI3617.1.

Langenbrunner, B. and Neelin, J.D. (2013) Analyzing ENSO Teleconnections in CMIP Models as a Measure of Model Fidelity in Simulating Precipitation. *Journal of Climate*, 26(13), 4431–4446. https://doi.org/10.1175/JCLI-D-12-00542.1.

Larsen, J.N., Anisimov, O.A., Constable, A., Hollowed, A.B., Maynard, N., Prestrud, P., Prowse, T.D. and Stone, J.M.R. (2014) Polar regions. In: Barros, V.R., Field, C.B., Dokken, D.J., Mastrandrea, M.D., Mach, K.J., Bilir, T.E., Chatterjee, M., Ebi, K.L., Estrada, Y.O., Genova, R.C., Girma, B., Kissel, E.S., Levy, A.N., MacCracken, S., Mastrandrea, P.R. and White, L.L. (Eds.) *Climate Change 2014: Impacts, Adaptation, and Vulnerability. Part B: Regional Aspects. Contribution of Working Group II to the Fifth Assessment Report of the Intergovernmental Panel on Climate Change*. Cambridge, UK and New York, NY: Cambridge University Press, pp. 1567–1612.

Leathers, D.J., Yarnal, B. and Palecki, M.A. (1991) The Pacific/North American Teleconnection Pattern and United States Climate. Part I: Regional Temperature and Precipitation Associations. *Journal of Climate*, 4(5), 517–528. https://doi.org/10.1175/1520-0442(1991)004<0517:TPATPA>2.0.CO;2.

Lee, T. and McPhaden, M.J. (2010) Increasing intensity of El Niño in the central equatorial Pacific. *Geophysical Research Letters*, 37, L14603. https://doi.org/10.1029/2010GL044007.

Li, S., Hoerling, M.P., Peng, S. and Weickmann, K.M. (2006) The Annular Response to Tropical Pacific SST Forcing. *Journal of Climate*, 19(9), 1802–1819. https://doi.org/10.1175/JCLI3668.1.

Li, X., Holland, D.M., Gerber, E.P. and Yoo, C. (2015) Rossby Waves Mediate Impacts of Tropical Oceans on West Antarctic Atmospheric Circulation in Austral Winter. *Journal of Climate*, 28 (20), 8151–8164. https://doi.org/10.1175/JCLI-D-15-0113.1.

Li, Y. and Lau, N.C. (2012) Impact of ENSO on the Atmospheric Variability over the North Atlantic in Late Winter—Role of Transient Eddies. *Journal of Climate*, 25(1), 320–342. https://doi.org/10.1175/JCLI-D-11-00037.1.

Lim, E.-P., Hendon, H.H. and Rashid, H. (2013) Seasonal Predictability of the Southern Annular Mode due to Its Association with ENSO. *Journal of Climate*, 26(20), 8037–8054. https://doi.org/10.1175/JCLI-D-13-00006.1.

van Loon, H. and Madden, R.A. (1981) The Southern Oscillation. Part I: global associations with pressure and temperature in northern winter. *Monthly Weather Review*, 109(6), 1150–1162. https://doi.org/10.1175/1520–0493(1981)109.

Lu, J., Chen, G. and Frierson, D.M.W. (2008) Response of the Zonal Mean Atmospheric Circulation to El Niño versus Global Warming. *Journal of Climate*, 21(22), 5835–5851. https://doi.org/10.1175/2008JCLI2200.1.

Pohl, B., Fauchereau, N., Reason, C.J.C. and Rouault, M. (2010) Relationships between the Antarctic Oscillation, the Madden–Julian Oscillation, and ENSO, and Consequences for Rainfall Analysis. *Journal of Climate*, 23(2), 238–254. https://doi.org/10.1175/2009JCLI2443.1.

Rajagopalan, B., Kushnir, Y. and Tourre, Y. (1998) Observed decadal midlatitude and tropical Atlantic climate variability. *Geophysical Research Letters*, 25, 3967–3970.

Rayner, N.A., Parker, D.E., Horton, E.B., Folland, C.K., Alexander, L.V., Rowell, D.P., Kent, E.C. and Kaplan, A. (2003) Global analyses of sea surface temperature, sea ice, and night marine air temperature since the late Nineteenth century. *Journal of Geophysical Research*, 108(D14), 4407. https://doi.org/10.1029/2002JD002670.

Robertson, A.W., Mechoso, C.R. and Kim, Y.-J. (2000) The Influence of Atlantic Sea Surface Temperature Anomalies on the North Atlantic Oscillation*. *Journal of Climate*, 13(1), 122–138. https://doi.org/10.1175/1520-0442(2000)013<0122:tioass>2.0.co;2.

Sanabria, J., Bourrel, L., Dewitte, B., Frappart, F., Rau, P., Solis, O. and Labat, D. (2018) Rainfall along the coast of Peru during strong El Niño events. *International Journal of Climatology*, 38(4), 1737–1747. https://doi.org/10.1002/joc.5292.

Santoso, A., McPhaden, M.J. and Cai, W. (2017) The defining characteristics of ENSO extremes and the strong 2015/2016 El Niño. *Reviews of Geophysics*, 55, 1079–1129.

Saravanan, R. and Chang, P. (2000) Interaction between tropical Atlantic variability and El Niño–Southern Oscillation. *Journal of Climate*, 13, 2177–2194. https://doi.org/10.1175/1520-0442(2000)013<2177:IBTAVA>2.0.CO;2.

Schemm, S., Rivière, G., Ciasto, L.M. and Li, C. (2018) Extratropical Cyclogenesis Changes in Connection with Tropospheric ENSO Teleconnections to the North Atlantic: Role of Stationary and Transient Waves. *Journal of the Atmospheric Sciences*. 75(11), 3943–3964. https://doi.org/10.1175/JAS-D-17-0340.1.

Seager, R., Harnik, N., Kushnir, Y., Robinson, W. and Miller, J. (2003) Mechanisms of Hemispherically Symmetric Climate Variability. *Journal of Climate*, 16(18), 2960–2978. https://doi.org/10.1175/1520-0442(2003)016<2960:MOHSCV>2.0.CO;2.

Solomon, S., Haskins, J., Ivy, D.J. and Min, F. (2014) Fundamental differences between Arctic and Antarctic ozone depletion PNAS, 111(17), 6220–6225.

Stuecker, M.F. (2018) Revisiting the Pacific Meridional Mode. *Scientific Reports*, 8, 3216. https://doi.org/10.1038/s41598-018-21537-0.

Stuecker, M.F., Bitz, C.M. and Armour, K.C. (2017) Conditions leading to the unprecedented low Antarctic sea ice extent during the 2016 austral spring season. *Geophysical Research Letters*, 44, 9008–9019. https://doi.org/10.1002/2017GL074691.

Sulca, J., Takahashi, K., Espinoza, J.C., Vuille, M. and Lavado-Casimiro, W. (2017) Impacts of different ENSO flavors and tropical Pacific convection variability (ITCZ, SPCZ) on austral summer rainfall in South America, with a focus on Peru. *International Journal of Climatology*, 38, 420–435. https://doi.org/10.1002/joc.5185.

Takahashi, K. and Dewitte, B. (2016) Strong and moderate nonlinear El Niño regimes. *Climate Dynamics*, 46, 1627–1645.

Takahashi, K., Montecinos, A., Goubanova, K. and Dewitte, B. (2011) ENSO regimes: reinterpreting the canonical and Modoki El Niño. *Geophysical Research Letters*, 38(10), L10704. https://doi.org/10.1029/2011GL047364.

Taschetto, S.A., Ummenhofer, C.C., Stuecker, M.F., Dommenget, D., Ashok, K., Rodrigues, R.R. and Yeh, S.-W. (2020) ENSO atmospheric teleconnections. In: McPhaden, M.J., Santoso, A. and Cai, W. (Eds.) *El Niño Southern Oscillation in a Changing Climate. AGU Monograph*. Washington, D.C.: American Geophysical Union. https://doi.org/10.1002/9781119548164.ch14.

Taylor, K.E., Stouffer, R.J. and Meehl, G.A. (2012) An Overview of CMIP5 and the Experiment Design. *Bulletin of the American Meteorological Society*, 93(4), 485–498. https://doi.org/10.1175/BAMS-D-11-00094.1.

Thompson, D.W.J. and Wallace, J.M. (1998) The Arctic oscillation signature in the wintertime geopotential height and temperature fields. *Geophysical Research Letters*, 25(9), 1297–1300. https://doi.org/10.1029/98GL00950.

Thompson, D.W.J., Wallace, J.M. and Hegerl, G.C. (2000) Annular Modes in the Extratropical Circulation. Part II: Trends. *Journal of Climate*, 13(5), 1018–1036. https://doi.org/10.1175/1520-0442(2000)013<1018:AMITEC>2.0.CO;2.

Trenberth, K.E., Branstator, G.W., Karoly, D., Kumar, A., Lau, N.-C. and Ropelewski, C. (1998) Progress during TOGA in understanding and modeling global teleconnections associated with tropical sea surface temperatures. *Journal of Geophysical Research*, 103(C7), 14291–14324.

Yan, H., Zhu, Z., Wang, B., Zhang, K., Luo, J., Qian, Y. and Jiang, Y. (2021) Tropical African wildfire aerosols trigger teleconnections over mid-to-high latitudes of Northern Hemisphere in January. *Environmental Research Letters*, 16, 034025. https://doi.org/10.1088/1748-9326/abe433.

Yang, S., Li, Z., Yu, J.-Y., Hu, X., Dong, W. and He, S. (2018) El Niño–Southern Oscillation and its impact in the changing climate. *National Science Review*, 5(6), 840–857. https://doi.org/10.1093/nsr/nwy046.

Yeh, S.-W., Cai, W., Min, S.-K., McPhaden, M.J., Dommenget, D., Dewitte, B., Collins, M., Ashok, K., An, S.I., Yim, B.Y. and Kug, J.-S. (2018) ENSO atmospheric teleconnections and their response to greenhouse gas forcing. *Reviews of Geophysics*, 56, 185–206. https://doi.org/10.1002/2017RG000568.

Yeh, S.-W., Kug, J.-S., Dewitte, B., Kwon, M.-H., Kirtman, B.P. and Jin, F.-F. (2009) El Niño in a changing climate. *Nature*, 461, 511–514.

Zheleznova, I.V. and Gushchina, D.Y. (2016) Circulation anomalies in the atmospheric centers of action during the Eastern Pacific and Central Pacific El Niño. *Russian Meteorology and Hydrology*, 41 (11–12), 760–769. https://doi.org/10.3103/S1068373916110030.

Zheleznova, I.V. and Gushchina, D.Y. (2015) The response of global atmospheric circulation to two types of El Niño. *Russian Meteorology and Hydrology*, 40(3), 170–179. https://doi.org/10.3103/S1068373915030036.

Zhou, S. and Miller, A.J. (2005) The Interaction of the Madden–Julian Oscillation and the Arctic Oscillation. *Journal of Climate*, 18(1), 143–159.

Zhu, Y. and Wang, T. (2016) The relationship between the Arctic oscillation and ENSO as simulated by CCSM4. *Atmospheric and Oceanic Science Letters*, 9(3), 198–203. https://doi.org/10.1080/16742834.2016.1149287.

Zhu, Z. and Li, T. (2016) A new paradigm for continental U.S. summer rainfall variability: Asia–North America teleconnection. *Journal of Climate*, 29(20), 7313–7327. https://doi.org/10.1175/JCLI-D-16-0137.1.

Zhu, Z. and Li, T. (2018) Amplified contiguous United States summer rainfall variability induced by East Asian monsoon interdecadal change. *Climate Dynamics*, 50(9–10), 3523–3536. https://doi.org/10.1007/s00382-017-3821-8.

Zhu, Z., Lu, R., Yan, H., Li, W., Li, T. and He, J. (2020) Dynamic Origin of the Interannual Variability of West China Autumn Rainfall. *Journal of Climate*, 33(22), 9643–9652. https://doi.org/10.1175/JCLI-D-20-0097.1.

SUPPORTING INFORMATION

Additional supporting information may be found online in the Supporting Information section at the end of this article.

How to cite this article: Gushchina, D., Kolennikova, M., Dewitte, B., & Yeh, S.-W. (2022). On the relationship between ENSO diversity and the ENSO atmospheric teleconnection to high-latitudes. *International Journal of Climatology*, *42*(2), 1303–1325. https://doi.org/10.1002/joc.7304